To the Graduate Council:

I am submitting herewith a thesis written by Marc Anthony Matulich entitled "Fatigue Life Evaluation of the Holston River Bridge Floor Beams." I have examined the final copy of this thesis for form and content and recommend that it be accepted in partial fulfillment of the requirements for the degree of Master of Science, with a major in Civil Engineering.

David W. Goodpasture, Major Professor

We have read this thesis
and recommend its acceptance:

Accepted for the Council:

Associate Vice Chancellor
and Dean of The Graduate School

Fatigue Life Evaluation of the Holston River Bridge Floor Beams

A Thesis presented for the
Master of Science Degree at the
University of Tennessee at Knoxville

Marc Anthony Matulich

May 1995

Acknowledgment

I would first like to thank my major professor, Dr. David W. Goodpasture for his guidance and assistance in the analysis of the test data. I would like to thank Dr. Hal Deatherage for his insight into the interpretation of the data, as well as the review of this document and sitting on my committee. I would also like to thank Dr. Edwin Burdette for his time spent reviewing this document and sitting on my defense committee.

It is also to the Tennessee Department of Transportation for which I am indebted, since the TDOT provided the funding and opportunity for conducting this research.

Abstract

In January 1992, the outside girder of the east bound lane of the Holston River Bridge experienced a "full height tear through the flanges and web" due to fatigue failure (2), caused by out of plane distortion. The girder was subsequently jacked back into place and spliced.

The Department of Civil Engineering at the University of Tennessee has since been conducting a study of the fatigue life of the Holston River Bridge, funded by the Tennessee Department of Transportation. One of the primary purposes of the study was to establish stress ranges at critical details of the bridge superstructure and to predict the remaining fatigue life of the bridge using the stress range test data.

Since the remaining fatigue life of the bridge is a function of its individual structural members, each critical member was analyzed separately. The floor beams were selected primarily because of the coped flanges; a factor which would make the floor beams susceptible to fatigue cracking. It was the objective of this thesis to: 1) study the critical details on the floor beams for potential fatigue problems; 2) analyze the stress data; and 3) estimate the remaining fatigue life of the floor beams based on the current and estimated future usage. This thesis describes the data collection process, presents the information obtained, and provides an estimate of the remaining fatigue life of the bridge floor beams.

Table of Contents

Table of Contents - continued

List of Figures

List of Figures - continued

List of Figures - continued

List of Figures - continued

List of Tables

List of Symbols

Symbol	Description
AASHTO	American Association of State Highway and Transportation Officials
A	S-axis intercept of a log-log plot of an SN allowable design curve
ADT	Average Daily Traffic
ADTT	Average Daily Truck Traffic
b	Negative slope of log-log plot of S versus N curve
c	Distance from neutral axis to extreme fiber where stress is computed
d	S-axis intercept of a log-log plot of an SN curve
DOT	Department of Transportation
FB	Floor Beam
F_{sr}	Fatigue limit, allowable stress range on an SN curve, below which a detail will endure an unlimited number of cycles without developing fatigue cracks
I	Moment of inertia at section of beam according to subscript
I/c	Section modulus at a section of beam according to subscript
ksi	Thousand pounds per square inch
lbf	Pound Force
M	Bending moment about floor beam neutral axis
MCP	Mean Crossing Peak counting method
n_i	Number of stress cycles with range magnitude, S_{ri}
N_i	Fatigue Life corresponding to constant stress range, S_{ri}
N_p	Number of stress cycles experienced by the bridge to date
N_p'	Number of trucks experienced by the bridge to date
N_r	Remaining fatigue life (cycles)
N_t	Total fatigue life (cycles)

List of Symbols - continued

Symbol	Description
PADTT	Projected Average Daily Truck Traffic
PC	Personal Computer
psi	Pounds per square inch
RF	Rainflow counting method
R-M-C	Root Mean Cube - Miner's Rule
SCF(k)	Stress Concentration Factor
SN	Stress versus Number of cycles curve
S_{re}	Equivalent Stress Range
$S_{re,rmc}$	Equivalent Stress Range - root mean cube value
S_{ri}	Constant Stress Range
$S_{r, max}$	Maximum stress range
S_{95}	Stress range two standard deviations below mean on a log-log plot of an SN curve
T	Total number of truck crossings over the test period, t
t	Test period
TCS	Test Control Software
2-D	Two dimensional
2D	Truck with two axles and dual rear tires
3D	Truck with three axles
2S1	Two axle tractor trailer rig with a one axle trailer
2S2	Two axle tractor trailer rig with a two axle trailer
3S2	Three axle tractor trailer rig with a two axle trailer
DT	Three axle tractor trailer rig with two trailers
σ_{max}	Maximum stress(psi)

List of Symbols - continued

Symbol	Description
σ_{nom}	Nominal stress(psi)
α_i	Fraction of occurrence of stress range, S_{ri}

Chapter 1

Introduction

1.1 Bridge Description and History

The Holston River Bridge is located on Interstate 40 approximately four miles east of downtown Knoxville, Tennessee. The bridge is approximately 1193 feet in length and consists of eight spans. The spans vary in length from 100 to 240 feet (figure 1.1). The bridge superstructure consists of four continuous longitudinal girders. The girders are approximately 7.5 feet in depth at span two and decrease to 5.75 feet throughout the other spans. Within the 240 foot span, cross-frames at 22 feet on center provide lateral support and transfer load from the concrete deck to the girders. On the remaining spans transverse floor beams span between the girders. The cross frames and floor beams support stringers. The girders and stringers support a 7.5 inch ribbed concrete deck which acts compositely with the girders. The exterior girders have cantilever braces (outriggers) supporting an outside stringer which provides an additional traffic lane or shoulder (figure 1.2).

While the bridge was under construction, the design was changed to accommodate a potential increase in traffic. Cantilever braces were added to the exterior girders to provide room for an additional traffic lane. In January 1992, the outside girder of the east bound lane experienced a "full height tear through the flanges and web" due to fatigue failure (2), caused by out of plane distortion.

The girder was subsequently jacked back into place and spliced. Additional web and stiffener plates were added to the outside girder where the cantilever braces frame into the girder web.

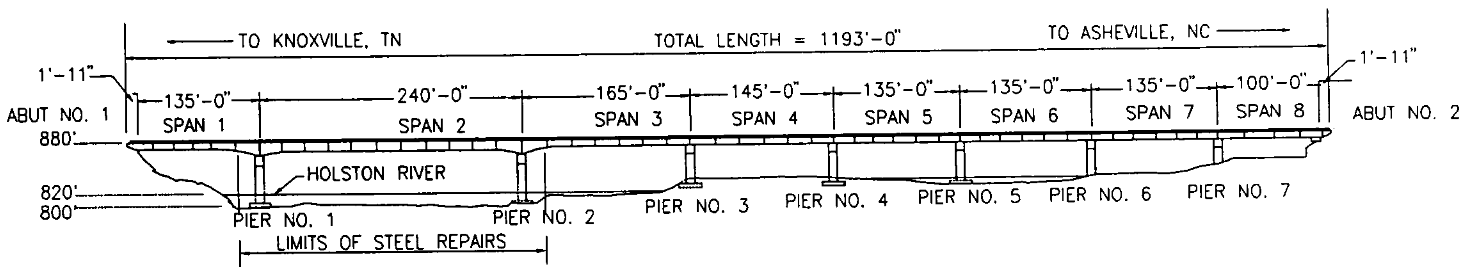

Figure 1.1. Holston River Bridge elevation view.

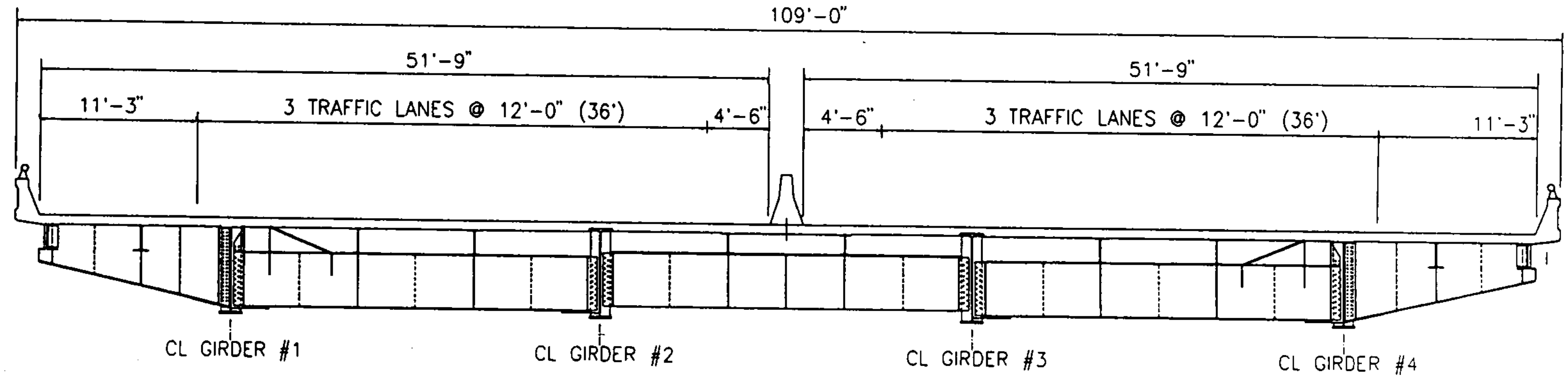

Figure 1.2 - Cross section of the Holston River Bridge at floor beam

1.2 Purpose of Research

Since August 1992, the Department of Civil Engineering at the University of Tennessee has been conducting a study of the fatigue life of the Holston River Bridge, funded by the Tennessee Department of Transportation. The purpose of the study was to: 1) identify controlling fatigue details; 2) determine the stress induced fatigue effects on the cross-frames, floor beams and main girders due to the retrofit repairs; 3) estimate the portion of the bridge fatigue life expended by the structure at the time of failure; and 4) estimate the remaining life of the bridge based on current and estimated future usage (2).

Since the remaining fatigue life of the bridge is a function of its individual structural members, each critical member must be analyzed separately. It was the objective of the work leading to this thesis to determine the stress history and the remaining fatigue life of the Holston River Bridge floor beams. This report describes the data collection process, presents the information obtained, and provides an estimate of the remaining fatigue life of the floor beams.

1.3 Methodology (2)

The methodology to obtain and analyze this information was as follows:

(A) Review of pertinent literature - A thorough review of literature was performed. This review consisted of obtaining information that would help in estimating the amount of fatigue experienced to date by the bridge.

(B) Location and installation of the strain gages - After reviewing the bridge plans and physically inspecting the bridge, with input from Dr. John Fisher, the locations of the critical members were determined. The members were then instrumented with strain gages at critical design details.

(C) Data Acquisition - After the gages were installed, field data were gathered for one hour intervals over a 48 hour period in July 1994. The data acquisition system used was the Optim Megadac data collection system. The Megadac system was connected to a Zenith personal computer that utilized the TCS 3000 software.

(D) Analysis of data during testing period - Two programs were created to separate and analyze the data. The results of these programs categorized the stress events at each strain gage. The data provided information relative to the magnitude and frequency of occurrence of the stresses in the bridge. These data were used to predict the remaining life of the bridge floor beams.

(E) Results and Conclusions - This thesis presents the results of the tasks above. It provides conclusions in the following areas:

1. Identification of potential fatigue problems at critical details on the floor beams from the dynamic response of the structure.

2. Analysis of the measured stress data obtained.

3. Estimated remaining fatigue life of the floor beam based on current and estimated future usage.

Chapter 2

Literature Review

2.1 Structural Fatigue

The fatigue life of a structural member is defined as "the length of time before an initially microscopic flaw in a critical structure detail develops into a crack of a certain length and becomes detectable by normal non-destructive inspection techniques" (8). The fatigue life is affected by a combination of factors. The most important considerations are the fatigue strength and type of structural detail, the magnitude of the stress ranges (live load and impact), loading history, and loading expectation (stress history).

2.2 Fatigue Strength and Types of Structural Details

If a repeated load is large enough to cause a fatigue crack, the crack will start at a point of maximum stress. This maximum stress is often due to a stress concentration. Stress concentrations can occur most often due to abrupt geometry changes in structural members (10). The effects of a geometry change (in this case a typical floor beam) on the stress distributions due to loadings are shown in figure 2.1.

As shown in figure 2.1, the coped flange causes an abrupt reduction in the section modulus (I/c) at section B of the beam. Since the geometry change is not gradual, a stress concentration is created with a maximum stress of magnitude σ_{max}.

It is difficult to determine the maximum stress, σ_{max}, at a stress concentration by theoretical analysis. It is also difficult to measure this stress, since it would require an infinitely small strain gage due to large stress gradients. However, it can be determined by applying a factor to the nominal stress obtained from the load-stress relationship of a

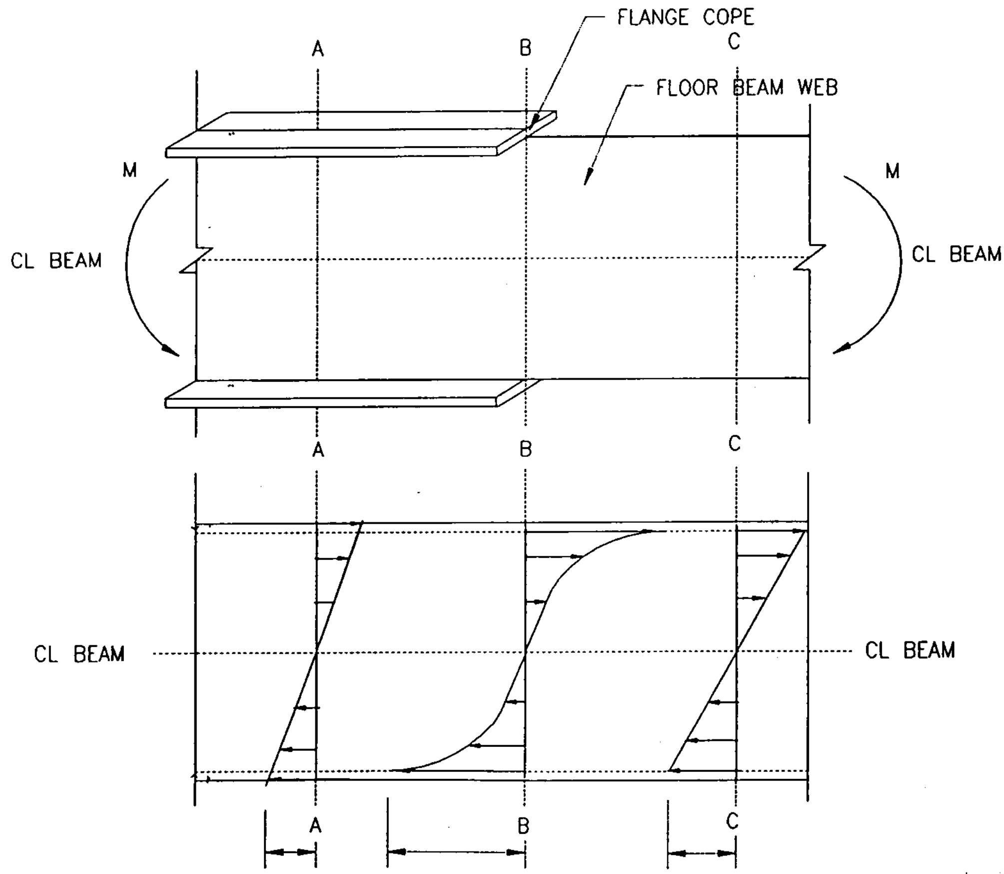

$$\sigma_A = \frac{Mc}{I_A} \qquad \sigma_B = \sigma_{MAX} = K\,\sigma_{NOM} \qquad \sigma_C = \sigma_{NOM} = \frac{Mc}{I_C}$$

Figure 2.1 Stress distributions of a typical floor beam with coped flanges subject to bending, M

particular detail. Such a factor is called a Stress Concentration Factor (SCF), k, and has been determined experimentally for many bridge structural details. The SCF is the ratio of the maximum stress to the nominal stress:

$$\text{SCF (k)} = \sigma_{max}/\sigma_{nom} = \text{maximum stress/ nominal stress}$$

Therefore, the estimation of the fatigue life of a detail can be determined from the measurement of the nominal stress range at the detail, σ_{nom}, and the experimental value of the SCF, k.

The fatigue life of a detail is based on experimental studies conducted at Lehigh University (5) and adopted by AASHTO (1). To account for the different degrees of stress concentration factors, different details are classified into eight detail categories, namely A, B, B', C, D, E, E', and F.

Each fatigue detail has a characteristic stress range versus cycle (SN) curve (figure 2.2), developed with data corresponding to test specimens subjected to zero-tension loading. The resulting test curves indicate the number of cycles, N, at a given stress range, S, required to bring the specimen to failure (also known as the Fatigue Strength). Category A represents details with the highest fatigue strength while category E' represents details with the lowest fatigue strength. Floor beams have a history of fatigue cracking and are usually classified as an E category, due to the flange terminations (copes).

The mean stress range, S, a member can sustain for a given number cycles, N, is given by the equation

$$NS^b = d \qquad \text{(equation 1)}$$

When plotted on a log-log scale, a straight line with an intercept d and a negative slope b is

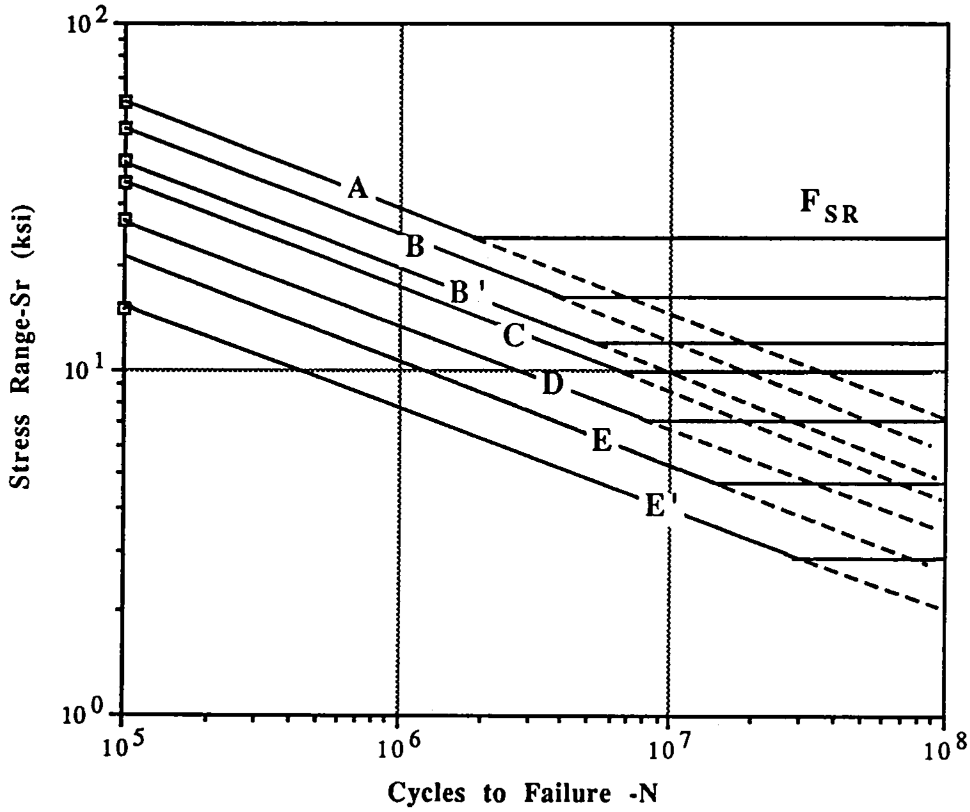

Figure 2.2 - AASHTO fatigue design curves for categories A to E'

obtained. There is considerable scatter in the fatigue data on which equation 1 is based, as shown in figure 2.3. Consequently, for design purposes the allowable nominal stress ranges are usually defined two standard deviations below the mean stress ranges, where

$$NS_{95}^{b} = A \qquad \text{(equation 2)}$$

in which A is the intercept for the allowable design curve and S_{95} is the stress range two-standard deviations below the mean (4).

For all detail categories, Fisher (5) proposed that the slope be taken as -3.0 and the intercept A is 20,000,000 cycles. The value of A and the slope of -3.0 defined the fatigue strength of each category and was the basis for the present AASHTO allowable fatigue stresses. Therefore, in the evaluation procedure the remaining fatigue life of a structural member is the remaining safe life when utilizing the AASHTO fatigue curves.

2.3 Determination of Stress Range Magnitude

To determine the amount of stress each fatigue prone detail experiences, an estimate of the stress range must be made. The SN curves are referenced to constant amplitude stress cycles. However, the stress cycles experienced by the actual bridge structural detail vary over a considerable range because of the variation of truck weights, truck configurations, truck speed, and location of the vehicles traversing the bridge relative to the location of the detail in question. Therefore, an equivalent constant amplitude stress range is used to assess the fatigue damage under variable range spectrum.

2.3.1 Equivalent Stress Range

Various methods have been used to arrive at a reasonable value for the equivalent constant amplitude stress range. Three such methods are as follows: the Single Truck Method, the AASHTO Design Stress Method and the Direct Measurement of Stress Range Method.

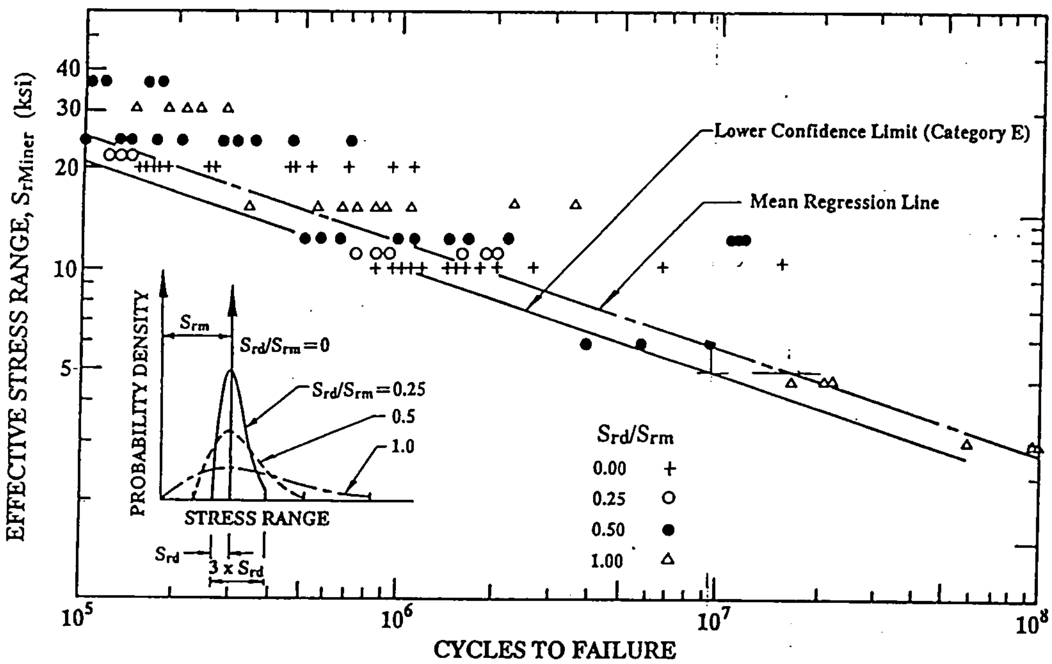

Figure 2.3 - Comparison of variable load tests with mean and lower confidence limits for a category E detail using Miner's Rule (reference 4)

The method used for a specific case is dependent upon site-specificity, effort, funding, and the degree of accuracy required.

The Single Truck Method is based on the observation that most of the stress cycles in a bridge structure are caused by single vehicle passages. Because a high percentage of the fatigue damage in a typical bridge in the United States is done by 4 and 5 axle semitrailers, the axle spacing and axle load distributions of the proposed "fatigue truck" approximate the spacing and load distribution for such trucks. "Fatigue Trucks" such as the HS-20 truck proposed by Fisher (8) and the HS-15 proposed by Moses et al (18) are aimed at a quick determination of an approximate value for the equivalent stress. Both take into account the infrequent occurrence of extreme stress ranges by relating the fatigue truck load to the variable load spectrum. Reference 18 lists details of the method.

The AASHTO Design Stress Method uses the AASHTO design live load and impact stress as the basis for fatigue evaluation. The method is explained in detail in reference 1. In general, the actual stress ranges in a structure are significantly lower than the live load and impact stresses predicted from the design method. In addition, this method does not distinguish between the maximum stress experienced by the detail, $S_{r,max}$, and the equivalent stress S_{re}; therefore this method leads to very conservative results (8).

The most site-specific and accurate method for stress range estimation is the Direct Measurement Method. It requires that fatigue prone details be instrumented with electrical resistance strain gages. The strains are monitored and recorded over a period of time which would realistically represent actual traffic patterns. A strain-time record resembles that of an influence line with superimposed strain fluctuations due to vibrations of the structure caused by moving loads (figure 2.4). A stress range spectrum (figure 2.5) is then

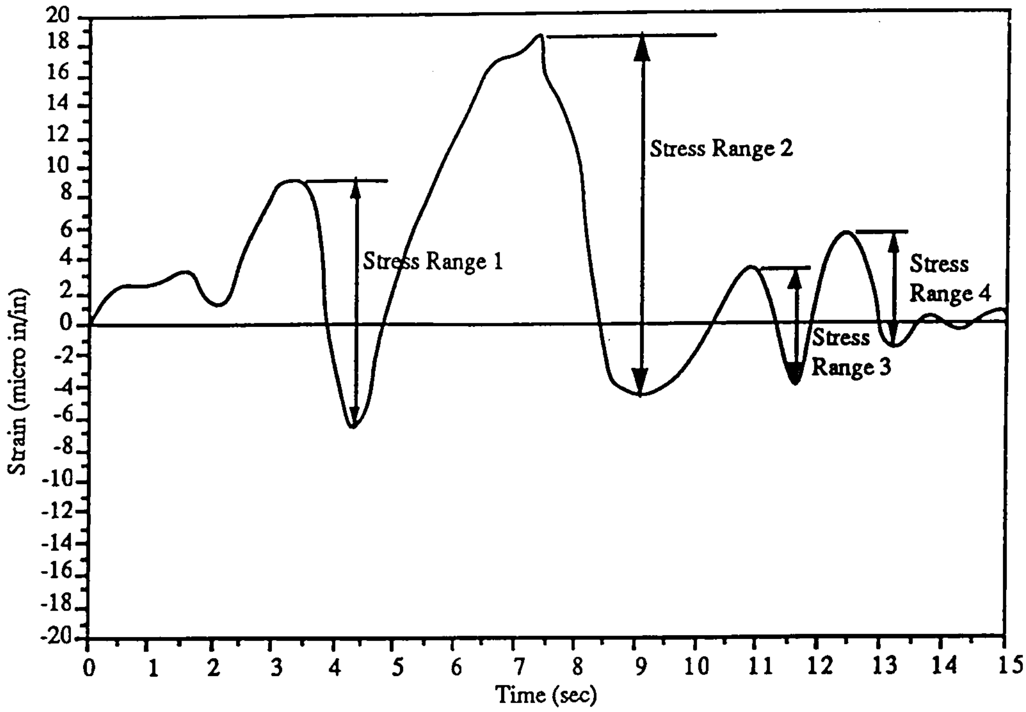

Figure 2.4. Typical strain-time record (reference 13)

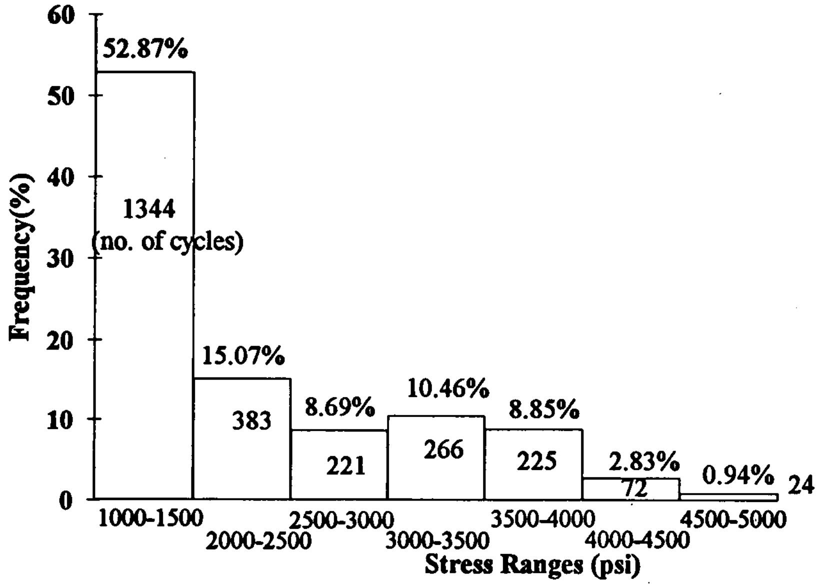

Figure 2.5 - Typical stress range spectrum

developed from the strain-time record, which shows the frequency of stress magnitudes over a period of time.

Bridge structures undergo many cycles of stress having many different magnitudes applied in a random manner. Miner's cumulative damage theory allows these factors to be considered when fatigue data are analyzed (17). In Miner's theory, it is hypothesized that if a material is subjected to n_i cycles at a constant stress-range level S_{ri}, where its expected fatigue life is N_i cycles, the fractional fatigue life used up is n_i/N_i. It is further assumed that, if a material is subjected to a stress range spectrum $S_{r1}, S_{r2}. S_{r3},...S_{ri},...$ and if the cycles are applied $n_1, n_2, n_3,..., n_i,...$ times at the respective stress range level, then fatigue failure will occur when

$$\sum n_i / N_i = 1 \qquad \text{(equation 3)}$$

where n_i = number of stress cycles with stress range magnitude, S_{ri}

and N_i = fatigue life corresponding to constant stress, S_{ri}

Since the slope of a typical SN curve for steel has a gradient of -1/3, the equivalent constant amplitude stress range based on Miner's theory is the "root-mean-cube" value of the variable stress ranges (17):

$$S_{re,rmc} = (\sum \alpha_i S_{ri}^3)^{1/3} \qquad \text{(equation 4)}$$

where $\alpha_i = \sum n_i / N_i$ = fraction of occurrence of constant stress range, S_{ri}.

Once the equivalent constant amplitude stress range (S_{re}) is calculated, the maximum stress range (S_{rmax}) is compared with the “fatigue limit” for that particular detail. The "fatigue limit" is defined as "the constant amplitude stress range below which the detail will be able to endure an unlimited number of cycles without developing fatigue cracks" (8). The "fatigue limits" of various details categories are specified in table 10.3.1.A of the AASHTO

Bridge Specifications, as the allowable stress range, Fsr, on an SN diagram (Figure 2.6). The "fatigue limit" of a category E detail is 4.5 ksi.

If all random variable stress ranges are below the fatigue limit, i.e., $S_{rmax} < F_{sr}$, cumulative fatigue damage will not develop and fatigue life is infinite.

If $S_{rmax} > F_{sr}$, fatigue cracking is expected after a number of stress cycles and the total fatigue life is not unlimited. It is based on the equivalent stress range S_{re}, which may be less than F_{sr}. To estimate the fatigue life in this case the SN design curve is extended below F_{sr} and this extension is used to evaluate the total fatigue life. As shown in figure 2.6, N_t represents the total fatigue life.

2.4 Estimation of Stress History and Remaining Fatigue Life

In order to accurately estimate the remaining life, the stress history of the bridge must be determined. Past traffic history can be obtained from DOT traffic counts listed in DOT publications or from the traffic engineer's office. Present day traffic data can be obtained from an on-site survey. Future traffic projections can be determined using linear regression. Since historical information does not always exist for some bridges, reference 7 provides a Design Method which may be used if the Present Average Daily Traffic, the truck traffic percentage and a national average truck traffic growth rate of 4.5% is assumed.

Figure 2.7 depicts an example of the ADTT (Average Daily Truck Traffic) volume versus time based on available data. The area under the ADTT curve multiplied by 365 days/year represents the total number of trucks experienced by the bridge to date. Depending on the characteristics of the bridge and the vehicle type, each truck causes one or more stress cycles per truck crossing (8). Therefore, the number of stress cycles experienced by the

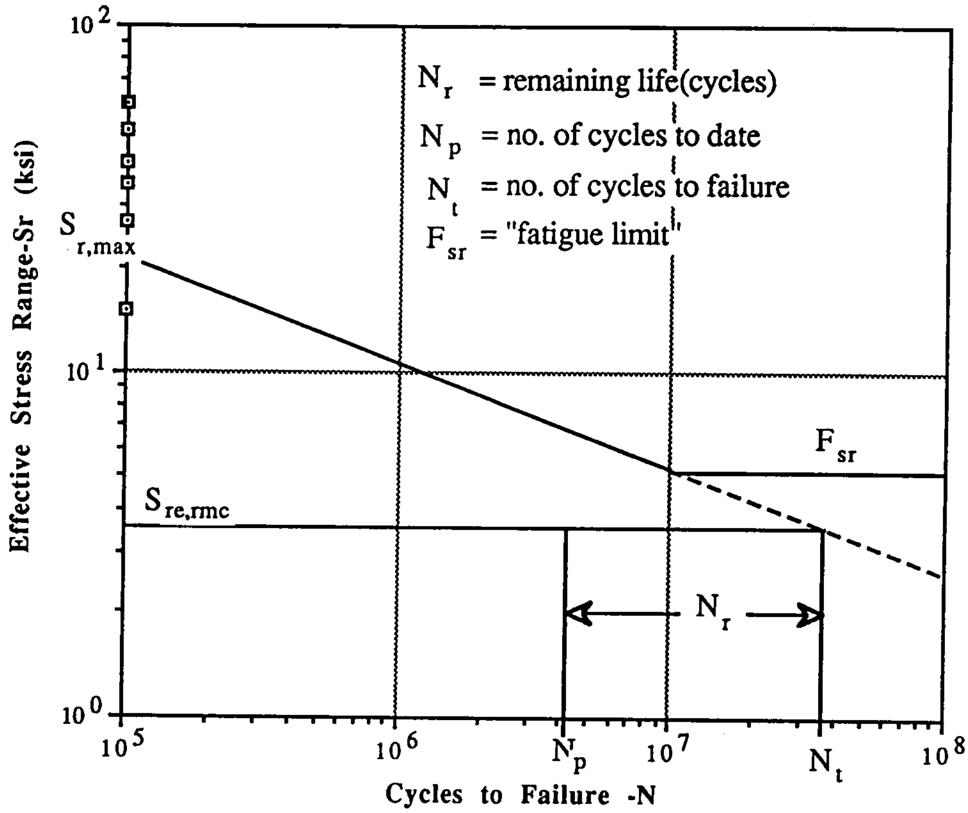

Figure 2.6 - Estimation of total fatigue life, Nt and remaining life, Nr

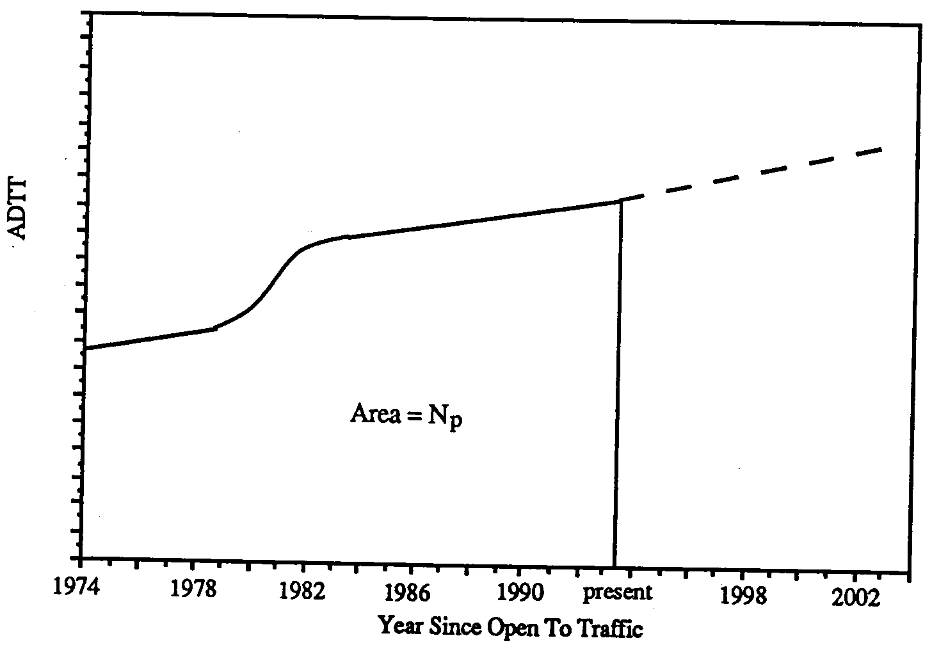

Figure 2.7 - Average Daily Truck Traffic (ADTT) variation with time (reference 13)

bridge to date, N_p, is calculated from the ADTT curve and an estimate of the number of stress cycles per truck, where

$$N_p(\text{cycles}) = N_p'(\text{trucks}) \times \text{Avg. cycles/truck}$$

The remaining fatigue life N_r is the difference between the total fatigue life of the member, N_t, and the cumulative fatigue damage experienced to date, N_p, i.e.,

$$N_r = N_t - N_p \qquad \text{(equation 5)}$$

The conversion of N_r into a length of time is dependent upon the projected ADTT curve, the average number of cycles per truck and the remaining fatigue life, N_r, where

$$\text{Remaining Life (yrs)} = \frac{N_r}{\text{PADTT} \times (\text{Avg. no. cycles/truck}) \times 365}$$

$$\text{and where the Avg. no. cycles/truck} = \frac{\sum n_i/\text{time(hr)}}{\text{no. trucks/time(hr)}} \qquad (16).$$

Chapter 3

Data Acquisition

3.1 Location of Strain Gages

After a review of the bridge plans and a physical inspection of the bridge with input from Dr. John Fisher, the locations of the strain gages on the floor beams were determined. These locations were based on details susceptible to fatigue and the development of stress concentrations.

The floor beams in span one were chosen to be instrumented for the study because its' design was typical of the other spans and it was easily accessible. Also, the floor beams in this span may possibly exhibit high stresses due to the impact loads, since it is adjacent to the bridge abutment.

From an examination of the floor beams, it was determined that the floor beam web-girder connections were areas of concern. Due to differential deflection of the girders, the partial fixity of the connections in conjunction with the coped floor beam flanges would cause high stresses near the flange weld toe. Therefore, six strain gages were placed on the floor beams as shown in figure 3.1. In order to more closely measure the nominal stress of the detail, the gages were placed a distance of two inches from the ends of the flanges in the vicinity of lower stress gradients. However, even at these locations the strains measured may still be affected by both the bending due to partial fixity and strain concentration at the flange weld toe.

A previous study (13) has indicated that a distance of two inches from the ends of the flanges is far enough so that the strain measured is not at the point of maximum stress and

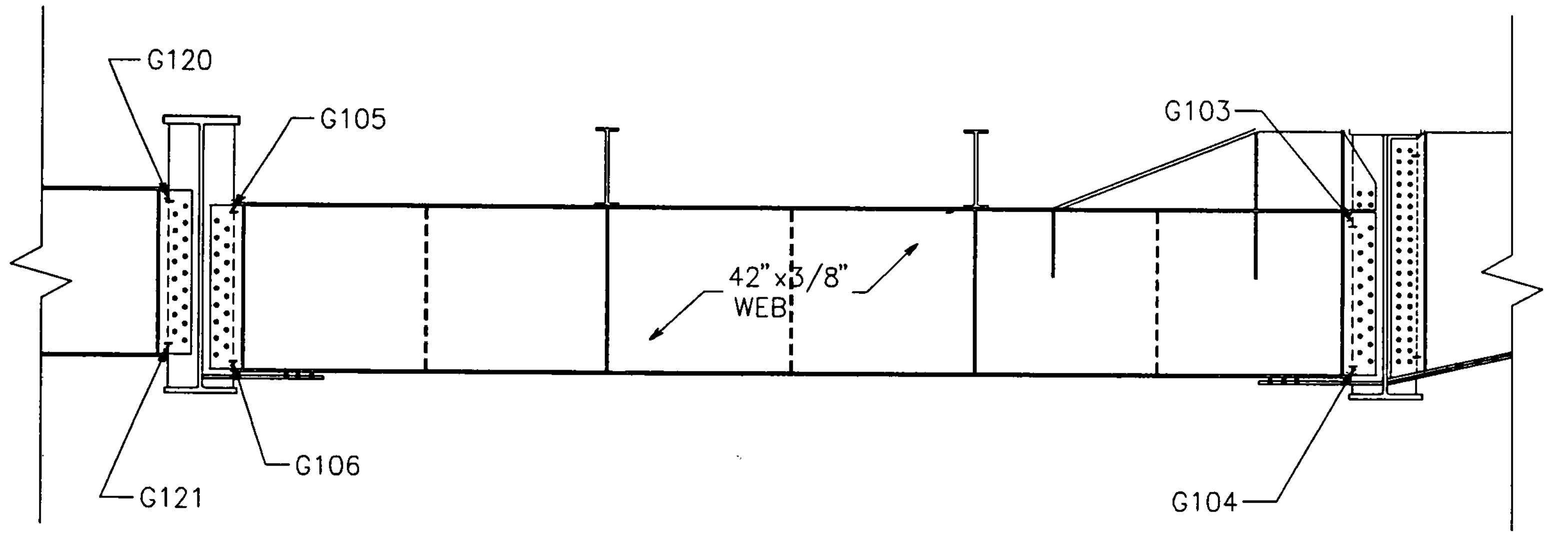

Notes: 1) ALL GAGES ARE 0.25 INCH E.R.S.G.
2) ALL GAGES ARE PLACED 1 INCH DOWN (FOR TOP COPE), UP (FOR BOTTOM COPE) AND 2 INCHES AWAY FROM THE COPED FLANGE WELD ROOT.

Figure 3.1 - Strain gage locations on floor beam.

is near enough so that measurements reflect the strain response at the end of the flange.

3.2 Stress Data Collection

3.2.1 Instrumentation

As discussed in the previous section, six electrical resistance foil strain gages were mounted on the floor beam as shown in figure 3.1. The gages used were of the 0.25 inch 350 ohm type manufactured by Micro-Measurements. The metal surfaces were stripped clean of paint and mill scale and the gages installed according to the manufacturer's instructions.

The system used for measuring the frequencies and magnitudes of strain range occurrences was the Optim Megadac system. Basically, the Megadac system consisted of a wheatstone bridge and modules (card types) which convert analog voltage signals from the strain gages into digital values. It has the capability to take measurements at a sampling rate of 25,000 samples per second, and had a capacity of 48 channels of input for the system used (19).

The Megadac was hooked up to an IBM personal computer (PC) installed with Optim's TCS (Test Control Software) package. TCS is a data base management package which defines the test parameters, definition of channels, calibration, recording and reviewing of test data. The Megadac could be triggered to start and stop the event measurements from the PC function key while using TCS.

During bridge testing, the sample rate was 50 samples per second. A total of 13 hours of data per strain gage was recorded over a 48 hour period at the bridge site. The measurements were recorded on the PC hard drive.

Data reduction programs were written to categorize the stresses seen by each gage. The programs analyzed and categorized the data according to two separate cycle counting methods, as discussed in the next section: the Mean Crossing Peak and Rainflow Methods. The MCP program logic is described in detail in reference 16.

3.2.2 Separation of Data and Cycle Counting Methods

The strain-time response data consisted of a variable amplitude loading situation which must be separated and evaluated in order to develop a stress spectrum. It was necessary to take the response data over a period of time and determine the number of cycles developed for a specific stress range caused by trucks.

Several methods have been developed and are in common use. The two methods used in this report are the Rainflow Counting and the Mean Crossing Peak methods. Basically, the Mean Crossing Peak method counts stress peaks and level crossings, while the Rainflow method counts stress ranges.

3.3.2.1 Rainflow Counting Method

The Rainflow method assumes plasticity at the crack tip and counts closed hysteresis loops on the strain diagram for the material in the plastic zone. The relationship between the strain-time plot and a stress-strain hysteresis plot at the crack tip where plasticity has developed is seen by comparing figures 3.2 and 3.3.

The stress-time curve can be seen to have three half-cycles a-d, d-e and e-f and one full cycle, b-c-b'. The same results are obtained by using the analogy of rain running down a series of roofs.

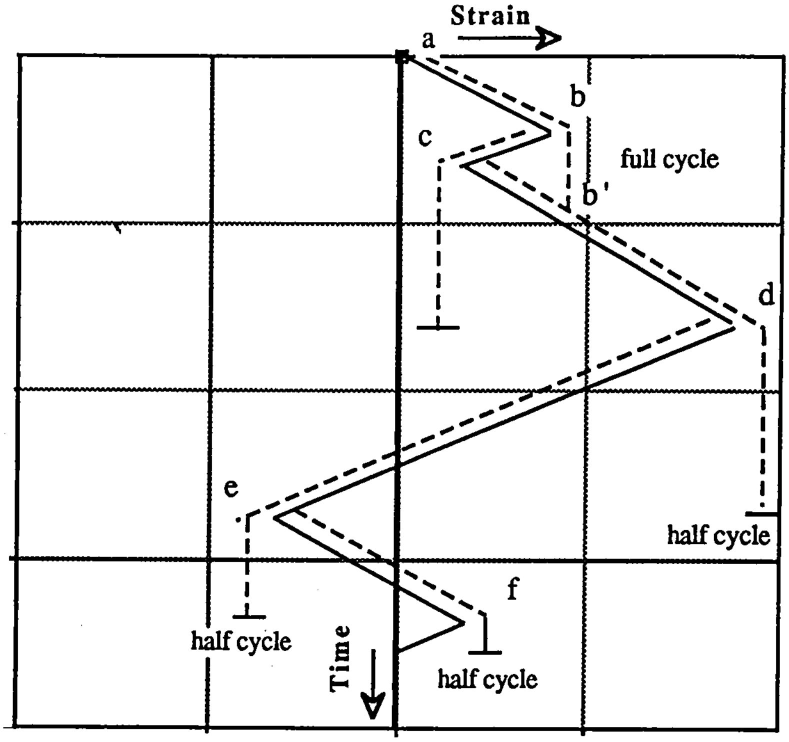

Figure 3.2 - Rainflow counting method for a simple strain-time plot

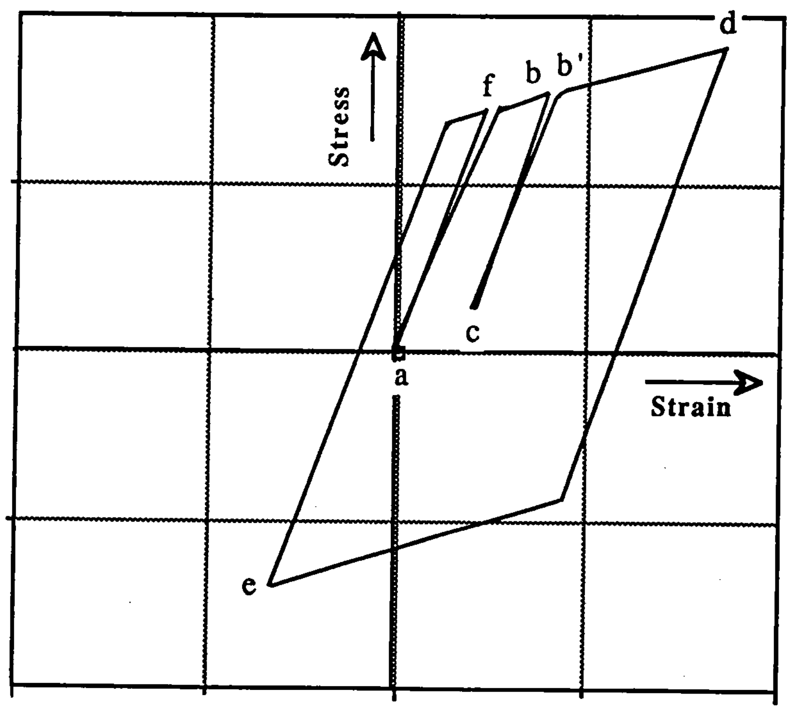

Figure 3.3 - Stress-strain hysteresis loop for a crack tip

The general rules for the Rainflow Counting method are as follows (4):

1. Rainflow begins at the beginning of the stress response and successively at the inside of every peak.

2. Flow initiating at a maximum drips down until it comes opposite a maximum more positive than the one from which it started. Flow initiating at a minimum drips down until it comes opposite a minimum more negative than the minimum from which it started.

3. Rain stops when it meets rain from the roof above.

4. The beginning of the sequence is a minimum if the initial straining is in tension.

5. The horizontal length of each rain flow is counted as a half cycle at that stress range.

In figure 3.3, rain (strain) initiates at a, flows to b, drips to b', flows to d, and finally stops opposite e, because e is more negative than a. Rain initiating at d flows to e and stops at the end of the record and flow initiating at e flows to f and stops at the end of the record. The number of cycles counted equals two and one half, resulting in a total of two and one half stress ranges.

3.3.2.2 Mean Crossing Peak Counting Method

The Mean Crossing Peak (MCP) method produces a mean (zero) axis, then counts the number of predetermined cycles that go above and below the mean axis. During testing the gage signal will drift. Therefore, as time passed during testing some cycles would not be counted that do not fall below the established zero axis. A data program was developed by Mayhew (16) which corrected for this problem by calculating the average of the first 20 and the last 20 data points; then it created a straight line between these two sets of twenty. That line was assumed to be the zero axis.

The program also checked to see if each data point was positive (indicating a crossing of the zero axis). The high and low strain data points were counted as a cycle, the times were recorded, and the strain difference was calculated. Stress was computed by multiplying the strain difference by Young's modulus for steel (29,000 ksi). The stress calculated was categorized and a stress spectrum developed. Details of the procedure are given in reference 16.

3.3 Test Results

A strain-time response curve of a 3S2 truck obtained during testing at gage 120 is shown in figure 3.4. It depicts the passage of the front axle and each of the tandem axles over the floor beam. In effect, the truck is moving from left to right, and the curve indicates the time that the axles cross the floor beam. The amplitude of the residual vibration after the truck has gone off the bridge was small in this test. However, in other tests, stress ranges of magnitude 500 psi and less appeared to be due more to instrumentation noise than significant loadings. Also, it is accepted practice to exclude stress magnitudes less than 1000 psi, since these stresses contribute very little to the effective stress range and are non-contributors to fatigue damage (10, 21). Therefore, once the stress ranges were categorized for both the Rainflow and MCP methods, any stress ranges less than 1000 psi were deleted from the spectrum. Periodically, a cycle of high magnitude occurred (15,000 psi). If the frequency of occurrence and the magnitude was determined to be a perturbation at the particular gage location, it was excluded from the spectrum.

From the 13 hours of test data, 5.75 hours were eliminated due to spontaneous axis drifts. Tables 3.1 and 3.2 show the results of test data accumulated for 7.25 hours from approximately 4329 trucks of the category 2D and larger using the Rainflow and MCP methods. Figures 3.5 through 3.12 show the stress range spectrums for each gage location that resulted from the two counting methods. A comparison indicates that the two

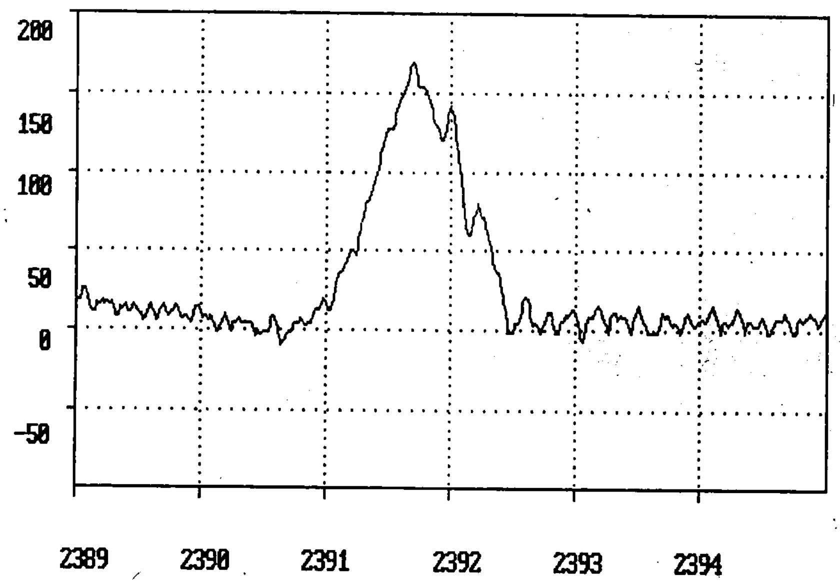

Figure 3.4. Typical strain-time response curve of a floor beam strain gage due to a 3S2 loading condition.

Table 3.1 - Estimated damage accumulation and effective stress range using the Rainflow method.

Rainflow Method								
Stress Range	Gage No.							
Sri(psi)	G105		G106*		G120		G121	
	No. Cycle	Freq.(%)	No. Cycle	Freq.(%)	No. Cycle	Freq.(%)	No. Cycle	Freq.(%)
1000-1500	1344	52.87	253	58.03	1821	41.30	1036	58.47
1500-2000	383	15.07	81	18.58	747	16.94	398	22.46
2000-2500	221	8.69	48	11.01	419	9.50	275	15.52
2500-3000	266	10.46	26	5.96	305	6.92	60	3.39
3000-3500	225	8.85	18	4.13	230	5.22	3	0.17
3500-4000	72	2.83	8	1.83	192	4.35	0	0.00
4000-4500	24	0.94	2	0.46	136	3.08	0	0.00
4500-5000	4	0.16	0	0.00	121	2.74	0	0.00
5000-5500	3	0.12	0	0.00	91	2.06	0	0.00
5500-6000	0	0.00	0	0.00	70	1.59	0	0.00
6000-6500	0	0.00	0	0.00	48	1.09	0	0.00
6500-7000	0	0.00	0	0.00	48	1.09	0	0.00
7000-7500	0	0.00	0	0.00	37	0.84	0	0.00
7500-8000	0	0.00	0	0.00	38	0.86	0	0.00
8000-8500	0	0.00	0	0.00	32	0.73	0	0.00
8500-9000	0	0.00	0	0.00	28	0.64	0	0.00
9000-9500	0	0.00	0	0.00	18	0.41	0	0.00
9500-10000	0	0.00	0	0.00	9	0.20	0	0.00
10000-10500	0	0.00	0	0.00	8	0.18	0	0.00
10500-11000	0	0.00	0	0.00	4	0.09	0	0.00
11000-11500	0	0.00	0	0.00	2	0.05	0	0.00
11500-12000	0	0.00	0	0.00	2	0.05	0	0.00
12000 - 12500	0	0.00	0	0.00	0	0.00	0	0.00
12500 - 13000	0	0.00	0	0.00	1	0.02	0	0.00
13000 - 13500	0	0.00	0	0.00	2	0.05	0	0.00
13500-14000	0	0.00	0	0.00	0	0.00	0	0.00
14000-14500	0	0.00	0	0.00	0	0.00	0	0.00
Time (hr)	7.25		5.20		7.25		7.25	
SUM(Sri>1000)	2542	100.00	436	100.00	4409	100.00	1772	100.00
Total no. trucks	4329		3407		4329		4329	
Sre(Sri>1000)	2196.90		1945.19		3728.30		1695.68	
Nt (cycles)	1.14E+08		1.65E+08		2.34E+07		2.49E+08	
Np(cycles)	3.21E+07		7.01E+06		7.04E+07		2.24E+07	
Nr (cycles)	8.23E+07		1.58E+08		-4.70E+07		2.26E+08	
Nr (years)	24		211		-8		95	

* Two hours of poor test data were deleted from the G106 results.

Table 3.2 - Estimated damage accumulation and effective stress range using the Mean Crossing Peak method

Mean Crossing Peak Method								
Stress Range	Gage No.							
Sri(psi)	G105		G106*		G120		G121	
	No. Cycle	Freq.(%)	No. Cycle	Freq.(%)	No. Cycle	Freq.(%)	No. Cycle	Freq.(%)
1000-1500	1414	42.15	349	58.66	1341	26.92	2113	75.79
1500-2000	653	19.46	159	26.72	765	15.36	523	18.76
2000-2500	531	15.83	77	12.94	486	9.76	138	4.95
2500-3000	513	15.29	9	1.51	506	10.16	14	0.50
3000-3500	202	6.02	1	0.17	448	8.99	0	0.00
3500-4000	33	0.98	0	0.00	454	9.11	0	0.00
4000-4500	9	0.27	0	0.00	317	6.36	0	0.00
4500-5000	0	0.00	0	0.00	231	4.64	0	0.00
5000-5500	0	0.00	0	0.00	156	3.13	0	0.00
5500-6000	0	0.00	0	0.00	97	1.95	0	0.00
6000-6500	0	0.00	0	0.00	58	1.16	0	0.00
6500-7000	0	0.00	0	0.00	41	0.82	0	0.00
7000-7500	0	0.00	0	0.00	30	0.60	0	0.00
7500-8000	0	0.00	0	0.00	12	0.24	0	0.00
8000-8500	0	0.00	0	0.00	14	0.28	0	0.00
8500-9000	0	0.00	0	0.00	14	0.28	0	0.00
9000-9500	0	0.00	0	0.00	6	0.12	0	0.00
9500-10000	0	0.00	0	0.00	5	0.10	0	0.00
10000-10500	0	0.00	0	0.00	1	0.02	0	0.00
10500-11000	0	0.00	0	0.00	0	0.00	0	0.00
11000-11500	0	0.00	0	0.00	0	0.00	0	0.00
11500-12000	0	0.00	0	0.00	0	0.00	0	0.00
12000 - 12500	0	0.00	0	0.00	0	0.00	0	0.00
12500 - 13000	0	0.00	0	0.00	0	0.00	0	0.00
13000 - 13500	0	0.00	0	0.00	0	0.00	0	0.00
13500-14000	0	0.00	0	0.00	0	0.00	0	0.00
14000-14500	0	0.00	0	0.00	0	0.00		0.00
Time(hrs)	7.25		5.20		7.25		7.25	
SUM(Sri>1000)	3355	100.00	595	100.00	4982	100.00	2788	100.00
Total no. trucks	4329		3407		4329		4329	
Sre(Sri>1000)	2128		1642		3554		1466	
Nt (cycles)	1.26E+08		2.74E+08		2.70E+07		3.85E+08	
Np(cycles)	4.24E+07		9.56E+06		6.30E+07		3.53E+07	
Nr (cycles)	8.34E+07		2.65E+08		-3.60E+07		3.49E+08	
Nr (years)	18		260		-5		93	

* Two hours of poor test data were deleted from the G106 results.

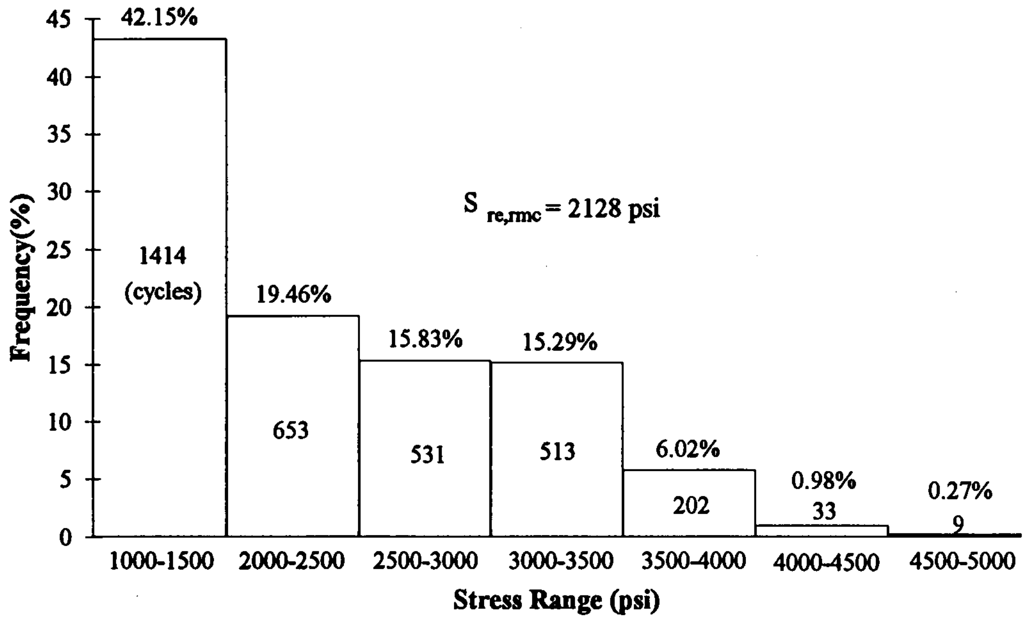

Figure 3.5 - Stress range spectrum for gage 105 using the Mean Crossing Peak counting method

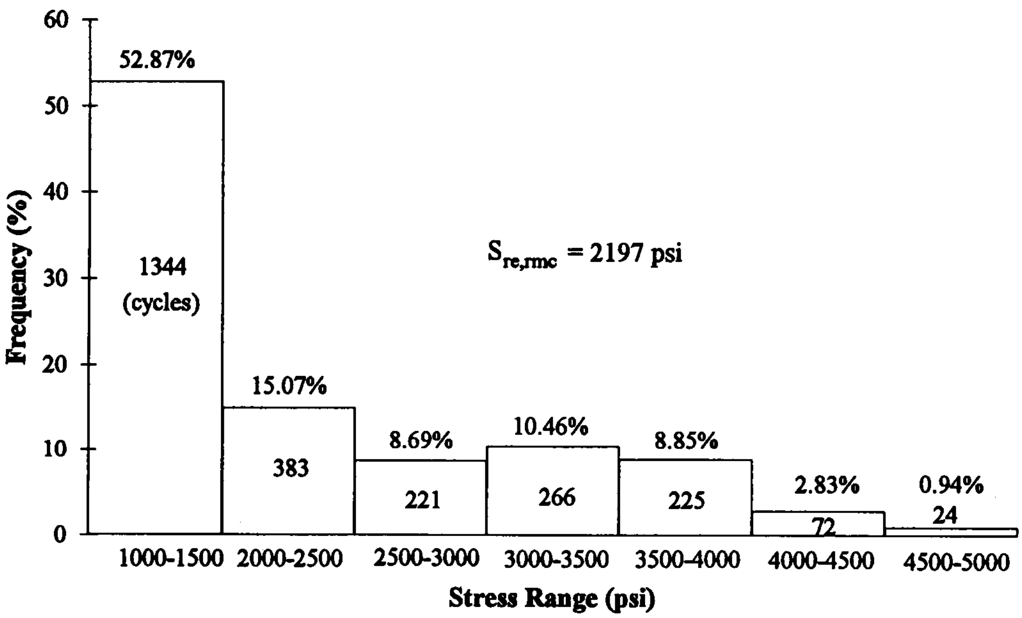

Figure 3.6 - Stress range spectrum for gage 105 using the Rainflow counting method

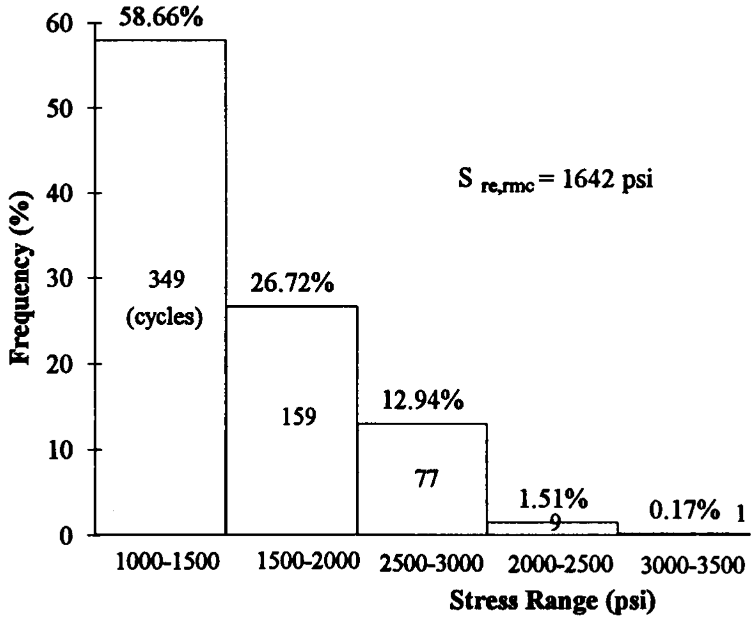

Figure 3.7 - Stress range spectrum for gage 106 using the Mean Crossing Peak counting method

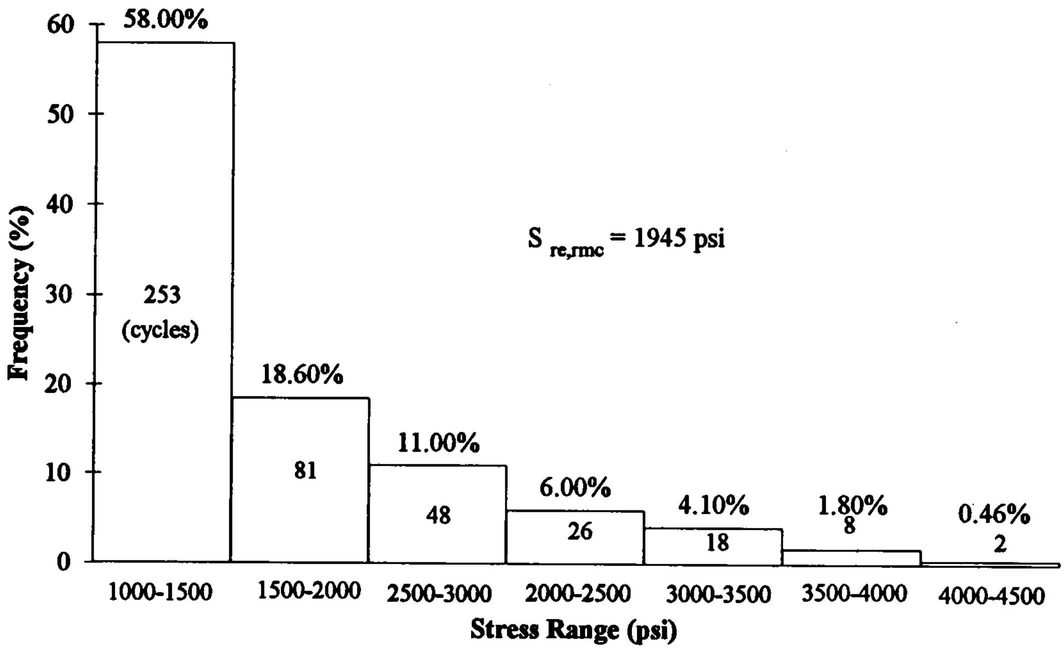

Figure 3.8 - Stress range spectrum for gage 106 using the Rainflow counting method

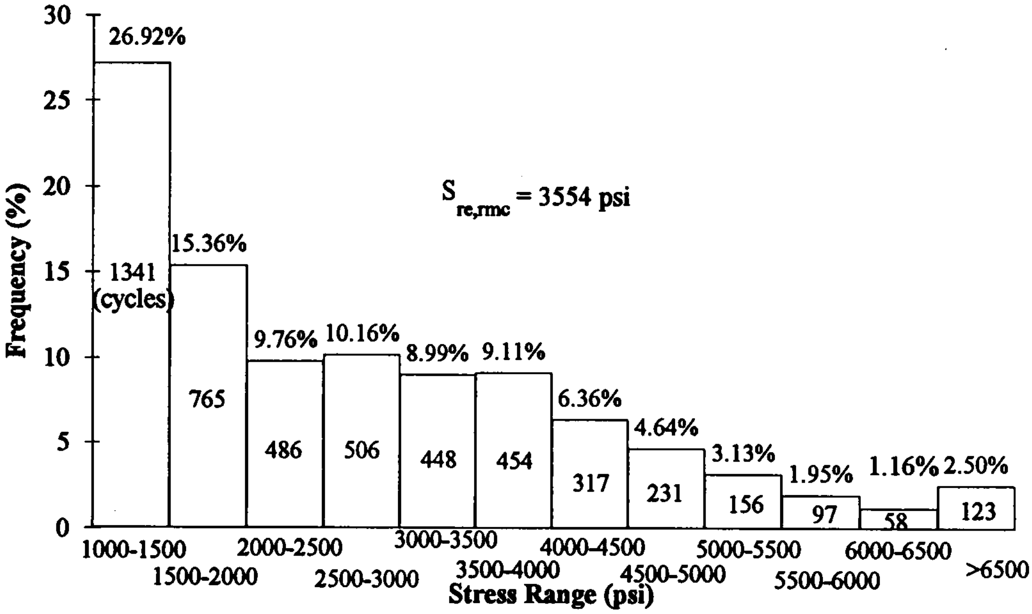

Figure 3.9 - Stress range spectrum for gage 120 using the Mean Crossing Peak counting method

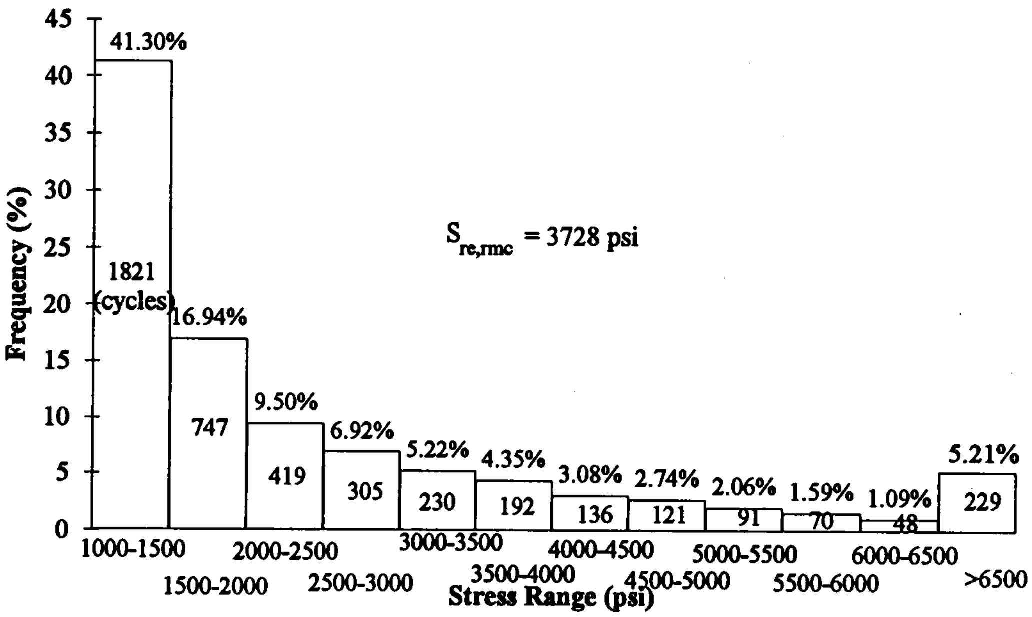

Figure 3.10 - Stress range spectrum for gage 120 using the Rainflow counting method

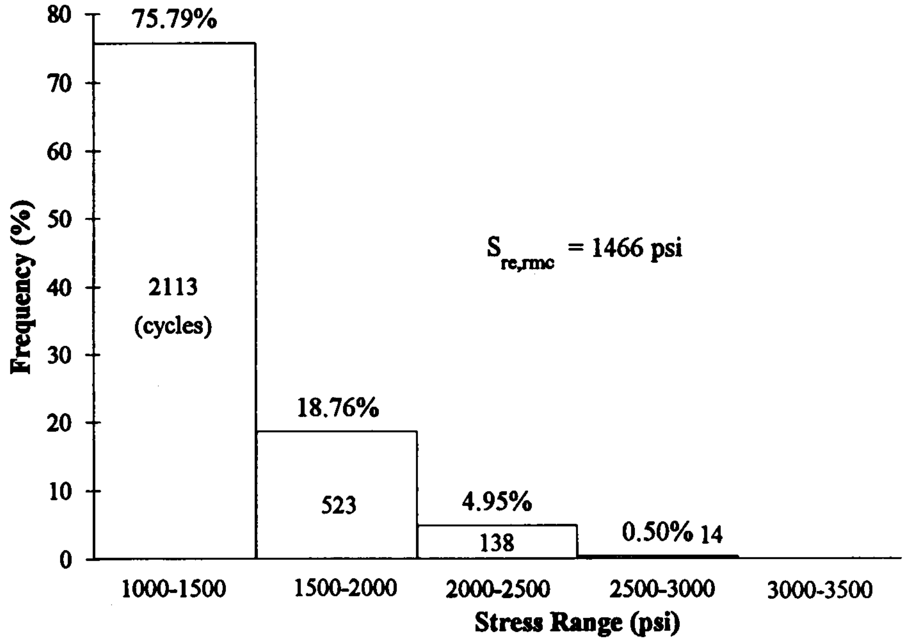

Figure 3.11 - Stress range spectrum for gage 121 using the Mean Crossing Peak counting method

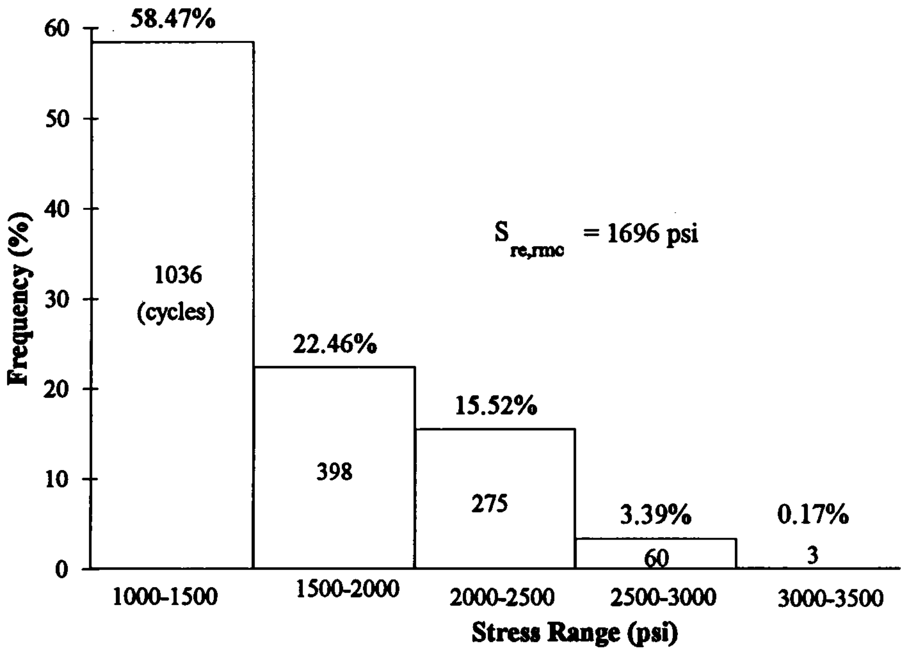

Figure 3.12 - Stress range spectrum for gage 121 using the Rainflow counting method

methods give approximately the same distribution from the test data. In all cases, more stress cycles resulted from the MCP counting procedure. Secondary stress cycles are accumulated to a much greater extent with Rainflow than with the Mean Crossing Peak Method (16). However, many of these cycles are less than 1000 psi; therefore, a bulk of the Rainflow cycles were deleted from the spectrum. This in turn increases the magnitude of the effective stress range. As a result, the two factors of decreased stress cycles and increased effective stress range tend to offset each other.

The data from gages 103 and 104 were not included in the data results since the stress responses were not significant enough to cause potential fatigue problems (i.e., less than 1000 psi).

3.4 Stress History

The bridge stress history was necessary to determine the number of significant loadings (stress cycles) the bridge has experienced to date. This information made possible an estimate of the probable remaining fatigue life due to present day traffic and predictions for future fatigue behavior should the traffic volume increase. The parameters required in the stress history estimation were the traffic volume and traffic characteristics on the bridge.

The assumption that pick-ups and other two axle vehicles were non-contributors to fatigue was verified while collecting the data. Therefore, only the truck volume history and truck traffic characteristics were estimated.

3.4.1 Truck Volume History and Truck Traffic Characteristics

The truck volume history was determined from the known Average Daily Traffic (ADT) counts taken approximately 1.5 miles east of the bridge site (reference 22) from prior years and applying factors to account for the truck traffic characteristics. Since the characteristics of the HRB were not recorded from years past, several assumptions were made: 1) the truck traffic characteristics of the HRB in 1974 were similar to that of West Knoxville bridges on I-40 in 1974; 2) the truck volume growth rate as a percentage of total traffic increased linearly from 1974 to the present; and 3) the projected truck volume growth will increase linearly. Based on these assumptions, the truck traffic over the HRB was determined as described in the following paragraphs.

The Average Daily Truck Traffic (ADTT) characteristics in prior years were determined from a previous study of West Knoxville bridges in 1976. The study was conducted by Goodpasture (9) in which the truck traffic was approximately 11% of the ADT based on an estimated 1974 ADT of 40,000 vehicles (figure 3.13) for a bridge located in West Knoxville on I-40. Since the assumption was made that the characteristics of the HRB in 1974 were similar to other Knoxville bridges in 1974, 11% of ADT was used as the truck traffic characteristics of the HRB in 1974.

The Present Average Daily Truck Traffic (PADTT) characteristics over the HRB were determined by a permanently installed counter located within 1.0 mile of the HRB. Data were taken over a five day period. The good data were separated and multiplied by appropriate seasonal factors. The results are shown in figure 3.14.

A comparison between figures 3.13 and 3.14 depicts an increase of 11% to 31.3% in ADTT as a percentage of total truck traffic over Knoxville Bridges. Furthermore, it shows an approximate increase from 46.4% to 86.8% ADTT in 3S2 trucks crossing the bridge.

Based on this information and the assumption of a linear truck volume growth rate, the

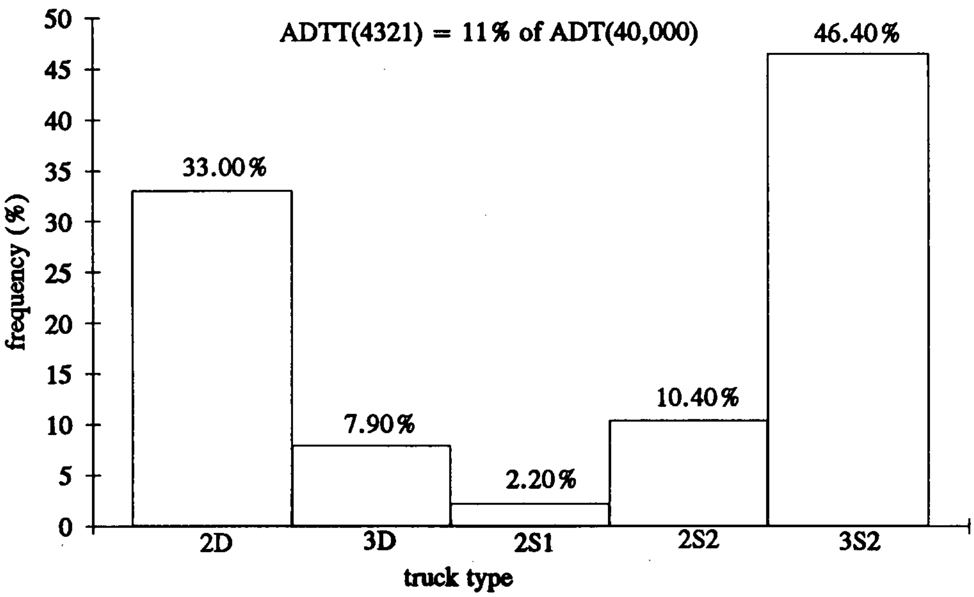

Figure 3.13 - Truck traffic characteristics of Knoxville bridges, 1974

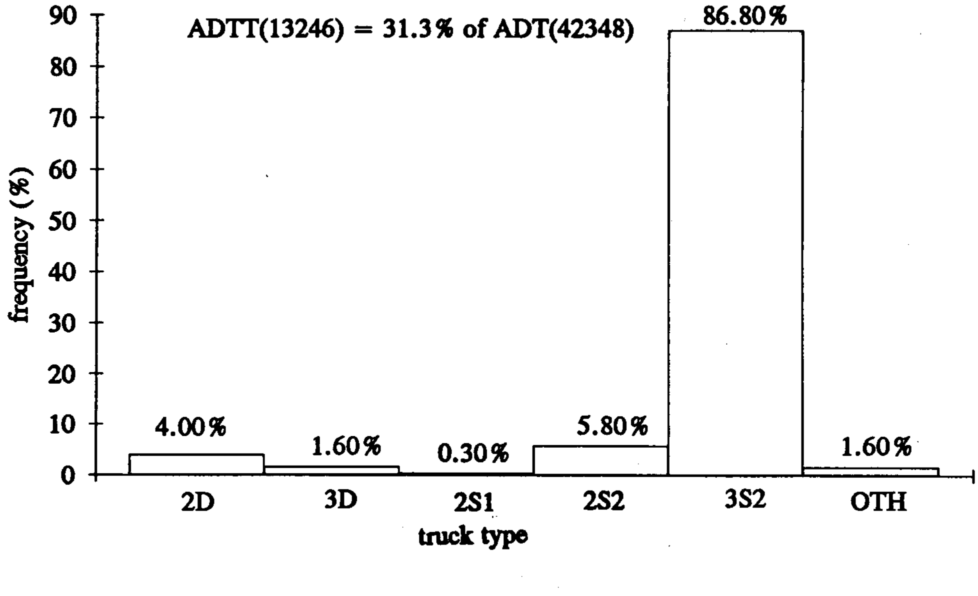

Figure 3.14 - Truck traffic characteristics of the Holston River Bridge, 1994

truck volume as a percentage of ADT was factored into the known ADT for each year from 1974 to 1994. From these data, a least squares linear regression analysis was performed to obtain the "best fit" curve. The resulting ADTT variation over time for the HRB is shown in figure 3.15. From this graph, the total number of trucks (east and west bound directions) the HRB has experienced to date (20 years) was estimated at 54,750,000 trucks.

3.4.2 Cycles Per Truck Passage

The correlation between fatigue cycles and truck traffic volume was determined by counting the number of trucks that crossed the bridge during the testing period versus the number of stress cycles computed for the test period. For each strain gage the number of cycles per truck was estimated from test data by,

$$\text{Avg. no. cycles/truck} = \Sigma ni \;/\; T$$

where

Σni = total number of stress cycles computed for the strain gage location over the test period, t

T = total number of truck crossings during test period, t.

The cumulative number of cycles the strain gage has experienced to date was then estimated from the equation,

$$N_p = \text{Avg. no. cycles/truck} \times 54{,}750{,}000 \text{ trucks}$$

The results for each strain gage location are tabulated in Tables 3.1 and 3.2.

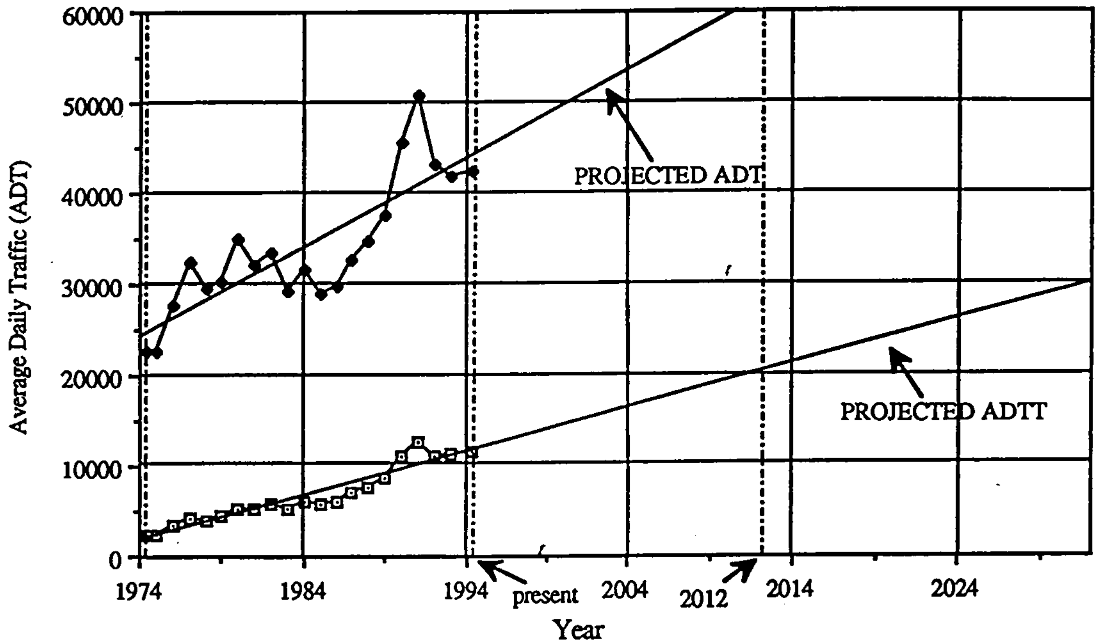

Figure 3.15 - Average Daily Traffic (ADT) and Average Daily Truck Traffic (ADTT) variation with time

Chapter 4

Interpretation of Data

4.1 Floor Beam Design and Behavior

Span one is located between the HRB abutment and pier one. Three floor beams run perpendicular to the longitudinal girders in this span and distribute the loads from the deck and stringers to the girders, in addition to providing lateral bracing and stability.

The floor beams each consist of a 3/8"x42" web fillet welded to 3/4"x9" top and bottom flanges (figure 4.1). Bearing stiffeners are located underneath the stringers and intermediate stiffeners are located at 4 foot intervals along the beam, which increase the strength of the web to carry shear. All material is A36 steel.

The floor beam web is connected to a transverse connection plate on the girder by seventeen 7/8 inch diameter high strength bolts (figure 4.2). To facilitate the attachment of the web to the transverse connection plate on the girders, the floor beam flanges were coped. The behavior of the coped flanges were of particular interest, since the coping causes an 80-90% reduction in bending resistance (4). The combination of coping and bending in the floor beams was expected to lead to stress concentrations and subsequent fatigue cracking. The copes were categorized as an AASHTO fatigue design detail Category E, which includes the ends of the longitudinal welds at the flange copes. On this detail, a fatigue crack was expected to initiate at the longitudinal weld toe termination of the flange cope and propagate into the web.

A gusset plate for lateral bracing is connected to the bottom flange of the outer floor beams and welded to the girder web (figure 4.1, Section A). The lateral bracing was designed to provide lateral stability to the bottom of the girder. The plate connection reduces the stress

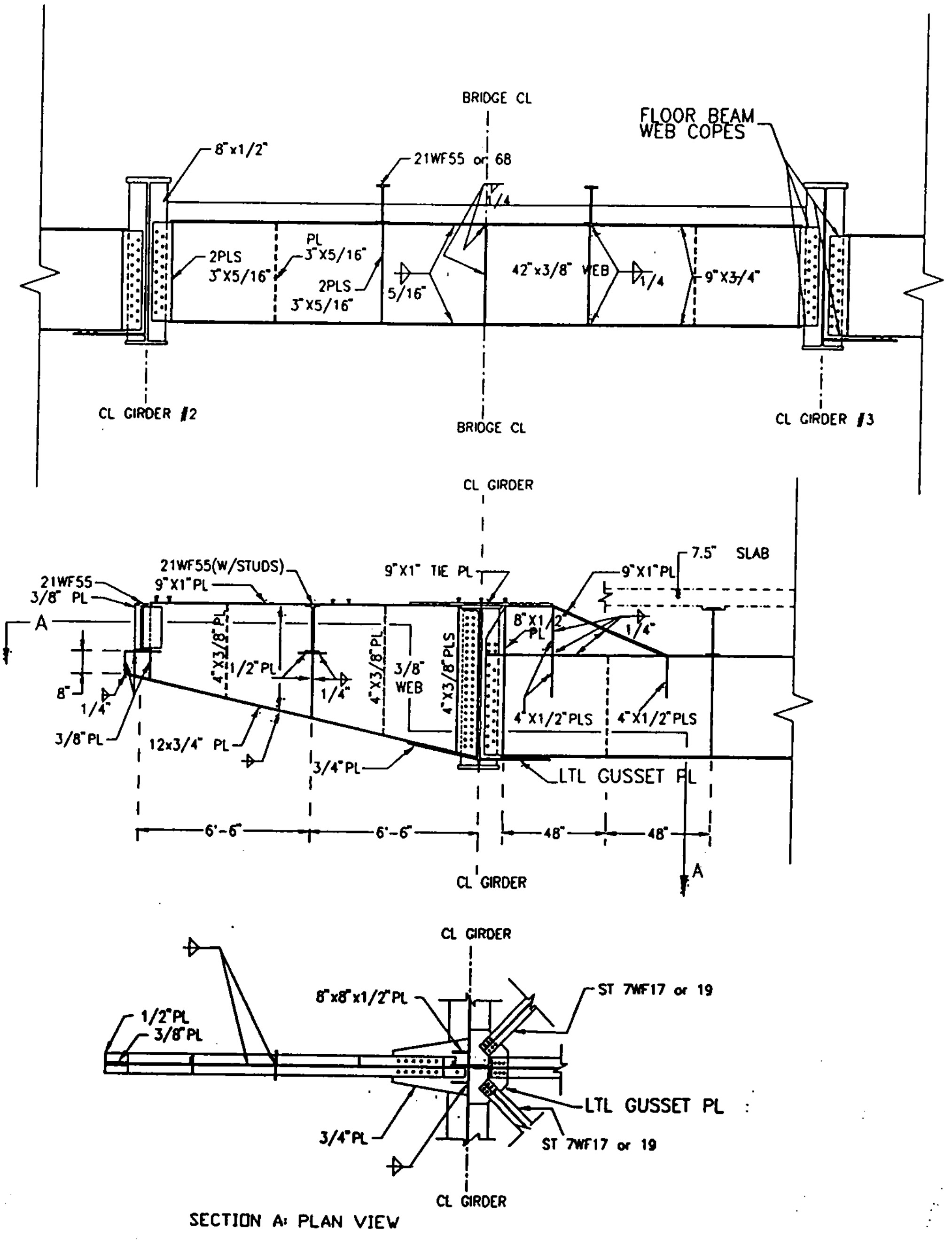

Figure 4.1 - Holston River Bridge floor beam detail

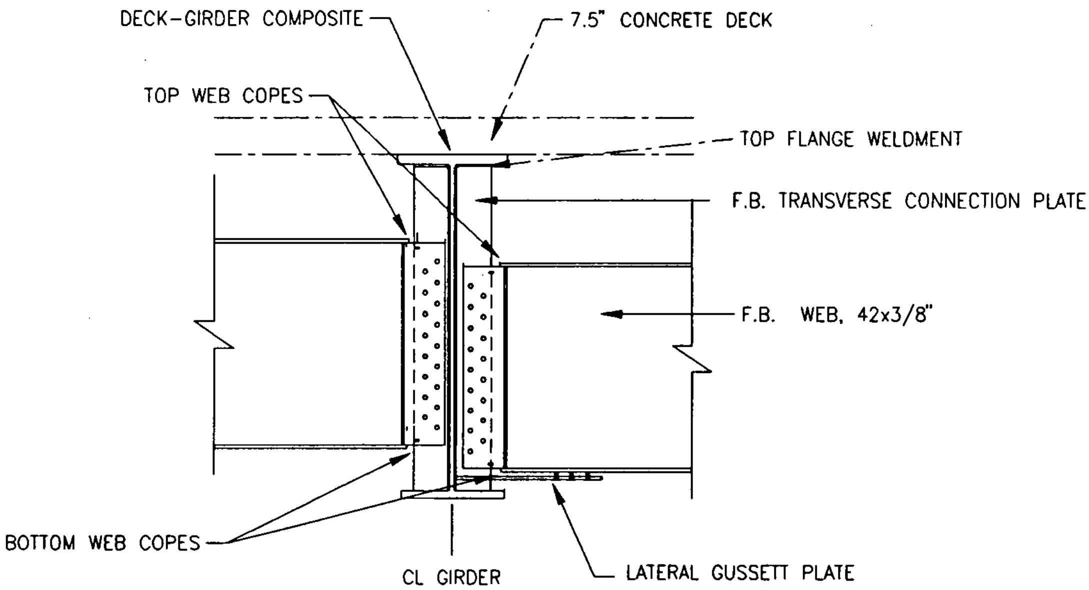

Figure 4.2 - Floor beam connection

in the floor beam bottom web cope, since some of the bending stress is transferred from the flange through the gusset plate to the girder web.

The deck and girder top flange act compositely and, therefore, are not susceptible to lateral displacement. The high end restraint due to this composite action was expected to cause greater stresses at the floor beam top web cope than the bottom web cope, since the embedded girder top flange resists the floor beam cyclic end rotation. Higher stresses were also expected in the top web cope, since the transverse connection plate was welded to the top girder flange and not to the bottom flange (figure 4.2).

Knee stiffeners are provided on the compression part of the outer floor beams adjacent to the outriggers. The stiffeners are designed to reduce out of plane distortion caused by the cantilever action of the outriggers. Even though the stiffeners will increase the end moment, M, of the floor beams, the section beam section modulus is significantly increased. Therefore, no significant stresses were expected in these locations.

4.2 Comparison of Measured versus Calculated Stresses on the Floor Beam

4.2.1 Measured Stresses

The strain responses were obtained at each of the gage locations due to a 3S2 truck in each of the lane loading conditions depicted in figure 4.3. The results are shown in figures 4.4 through 4.15, respectively. The strain responses were converted to stresses and tabulated in Table 4.1. The strain responses of gages 103 and 104 were not significant (i.e., less than 1000 psi) and, therefore, were not included in the Table.

4.2.2 Calculated Stresses

A two dimensional floor beam model (Appendix A) was used to interpret the measured

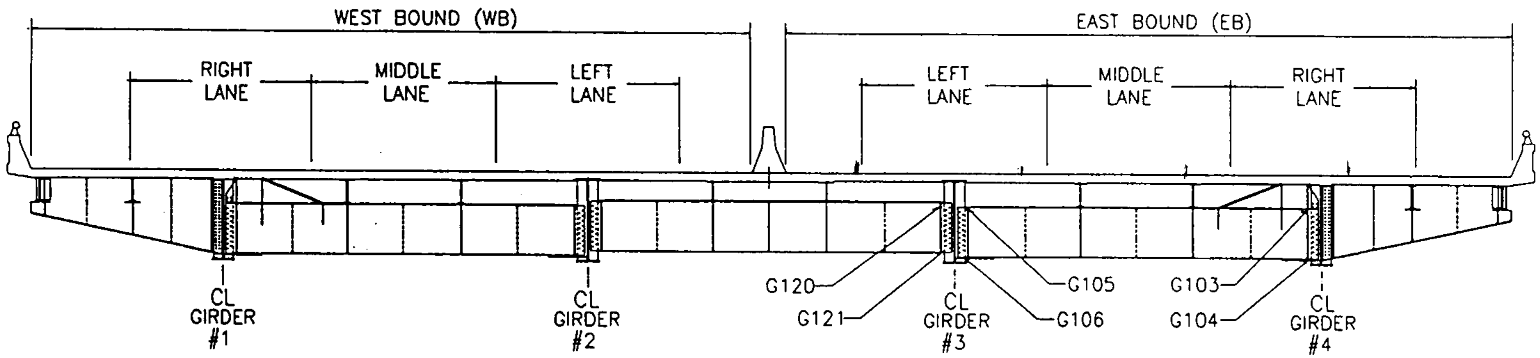

Figure 4.3 - Six lane loading conditions for the measured stresses

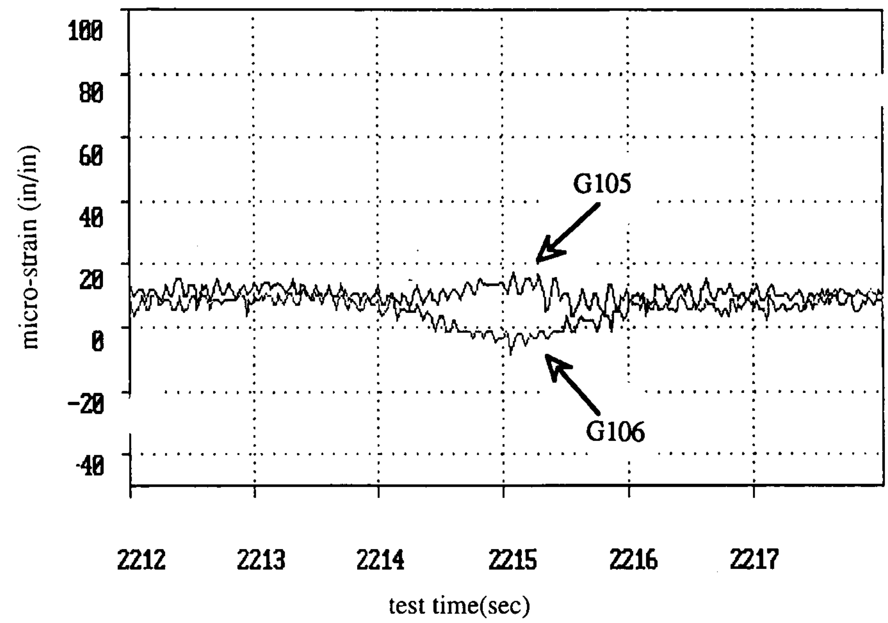

Figure 4.4 - Strain responses for gages 105 and 106 due to a 3S2 truck - west bound right lane

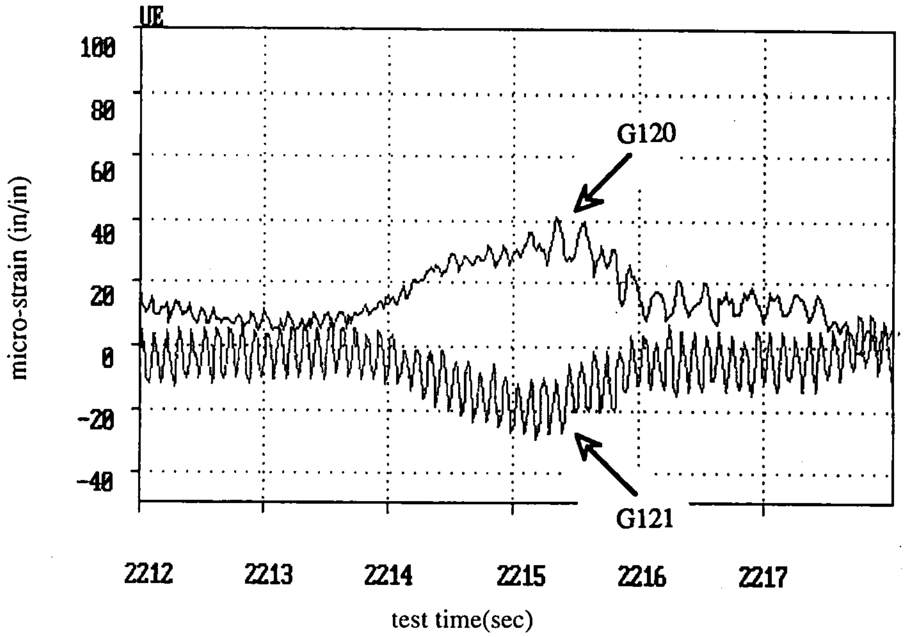

Figure 4.5 - Strain responses for gages 120 and 121 due to a 3S2 truck - west bound right lane

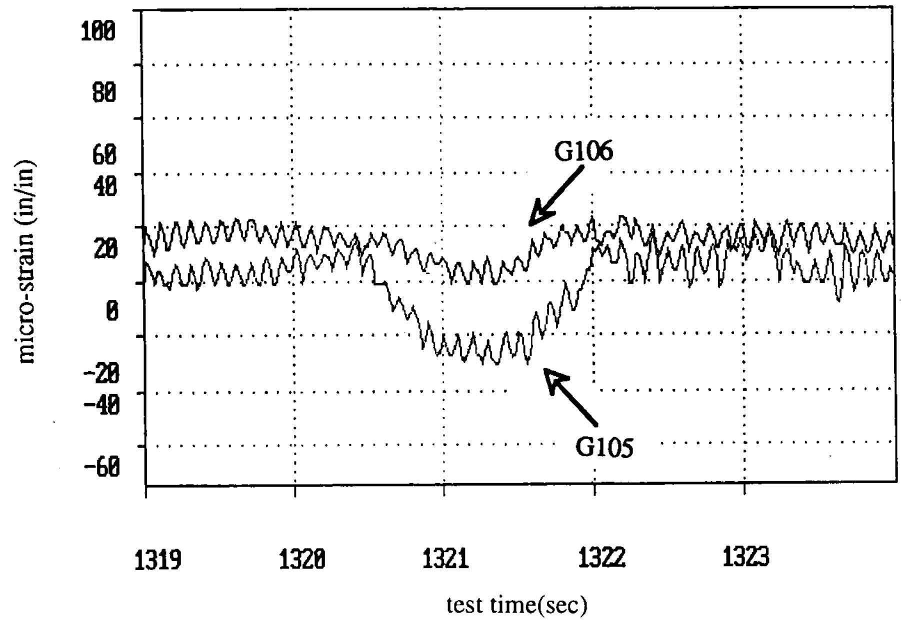

Figure 4.6 - Strain responses for gages 105 and 106 due to a 3S2 truck - west bound middle lane

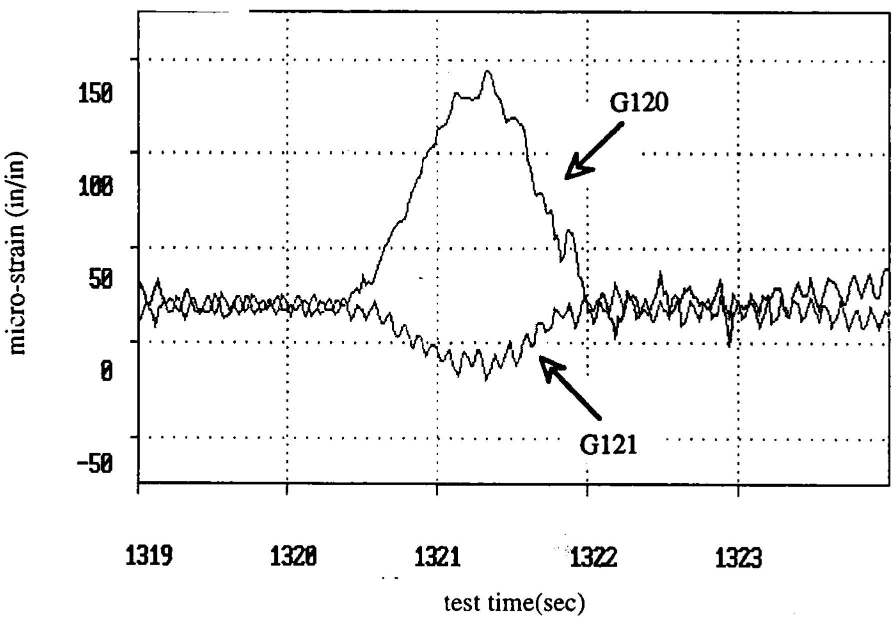

Figure 4.7 - Strain responses for gages 120 and 121 due to a 3S2 truck - west bound middle lane

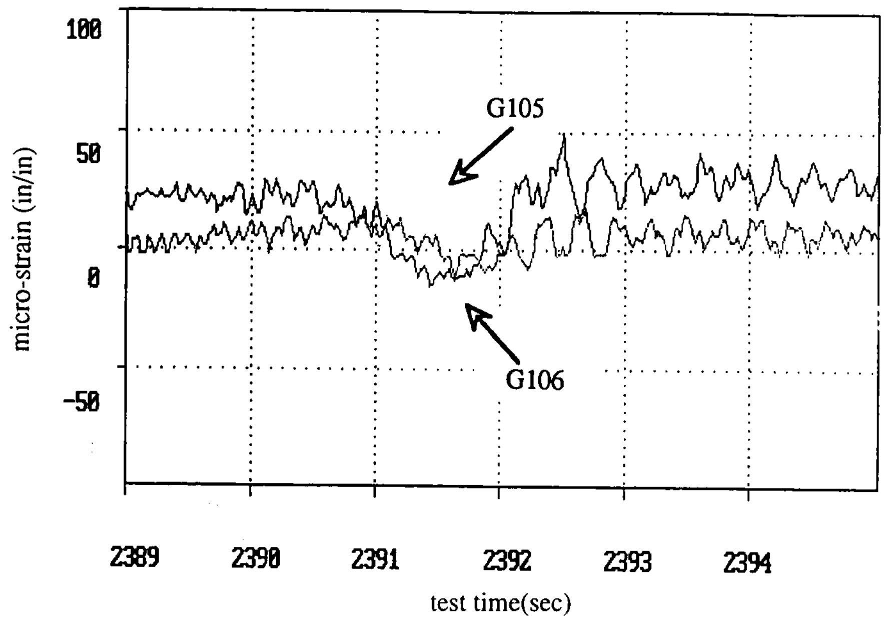

Figure 4.8 - Strain responses for gages 105 and 106 due to a 3S2 truck - west bound left lane

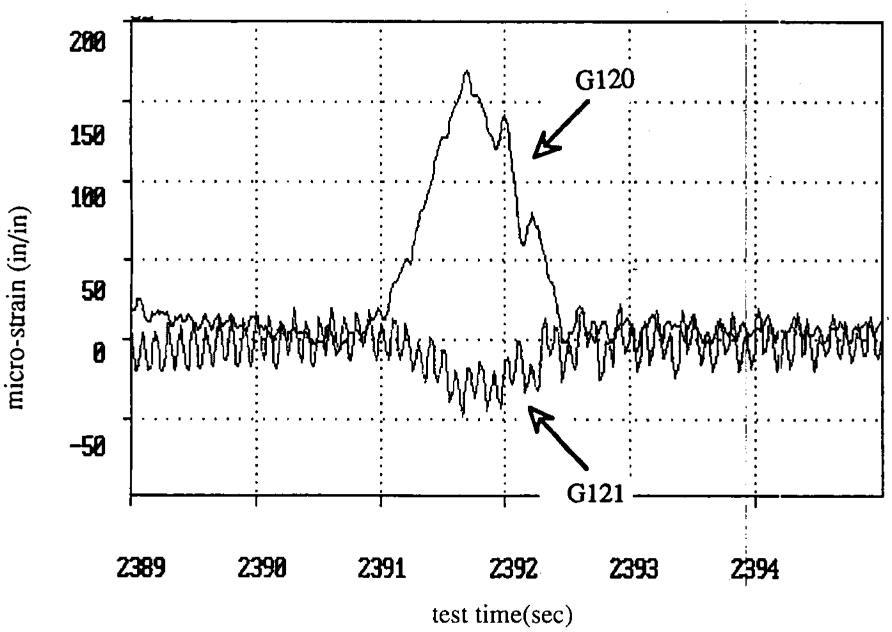

Figure 4.9 - Strain responses for gages 120 and 121 due to a 3S2 truck - west bound left lane

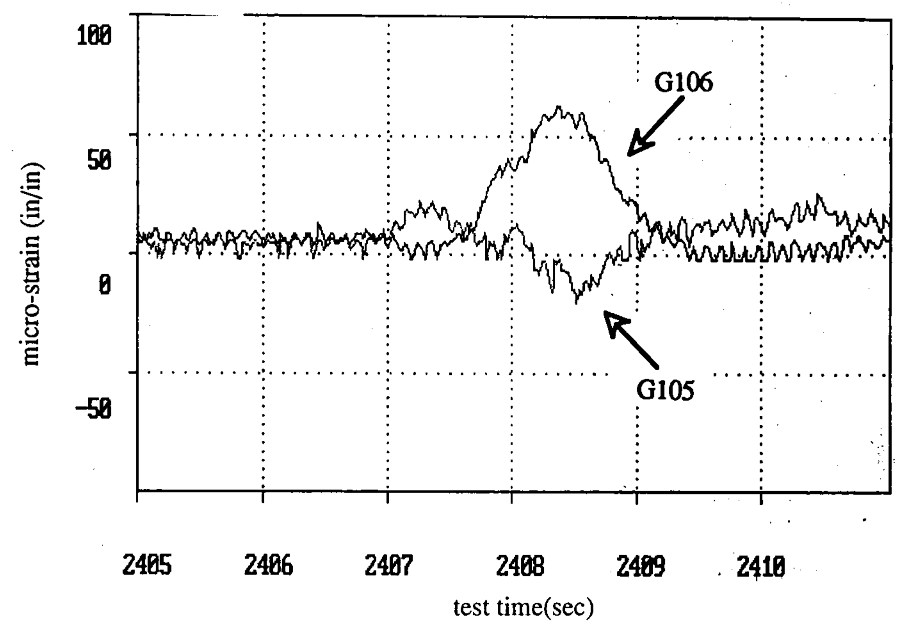

Figure 4.10 - Strain responses for gages 105 and 106 due to a 3S2 truck - east bound left lane

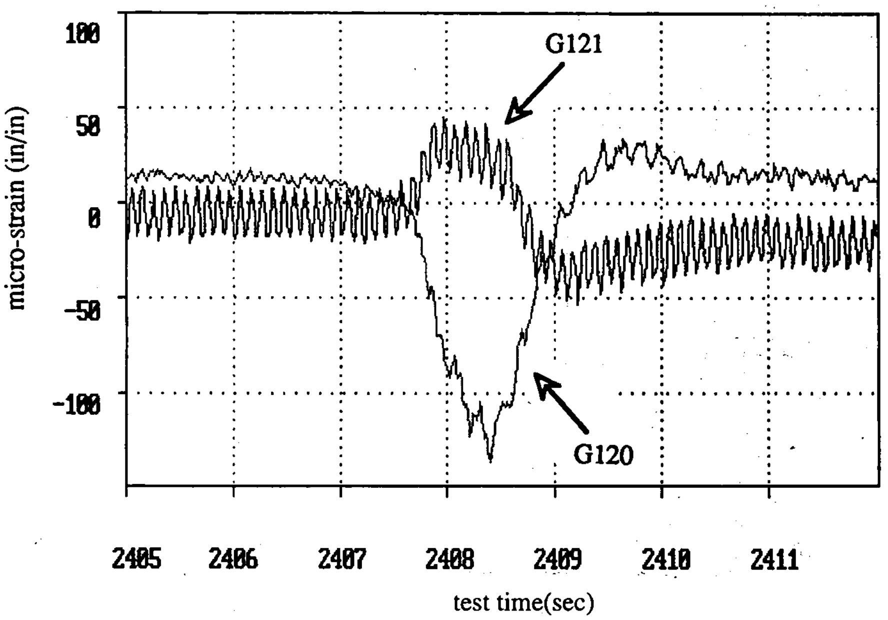

Figure 4.11 - Strain responses for gages 120 and 121 due to a 3S2 truck - west bound left lane

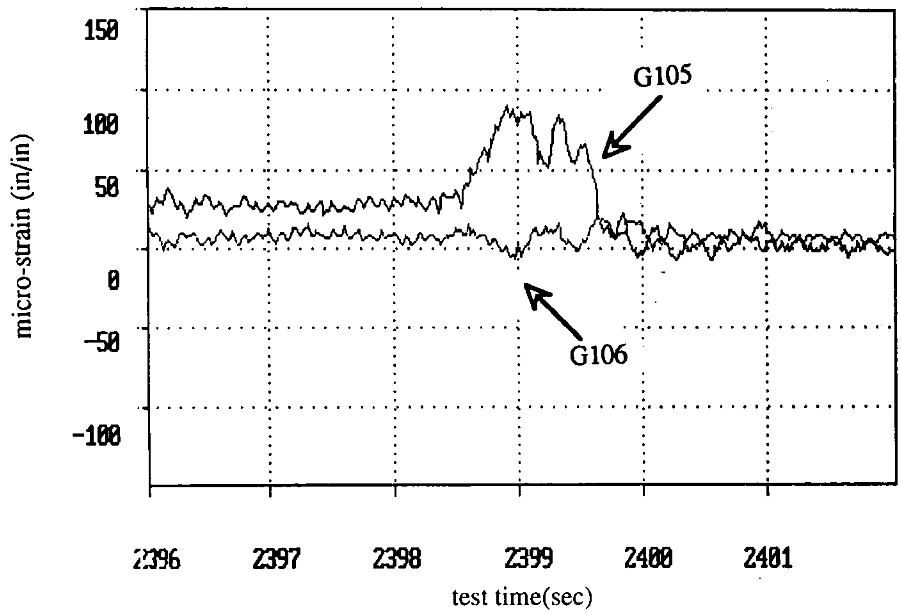

Figure 4.12 - Strain responses for gages 105 and 106 due to a 3S2 truck - east bound middle lane

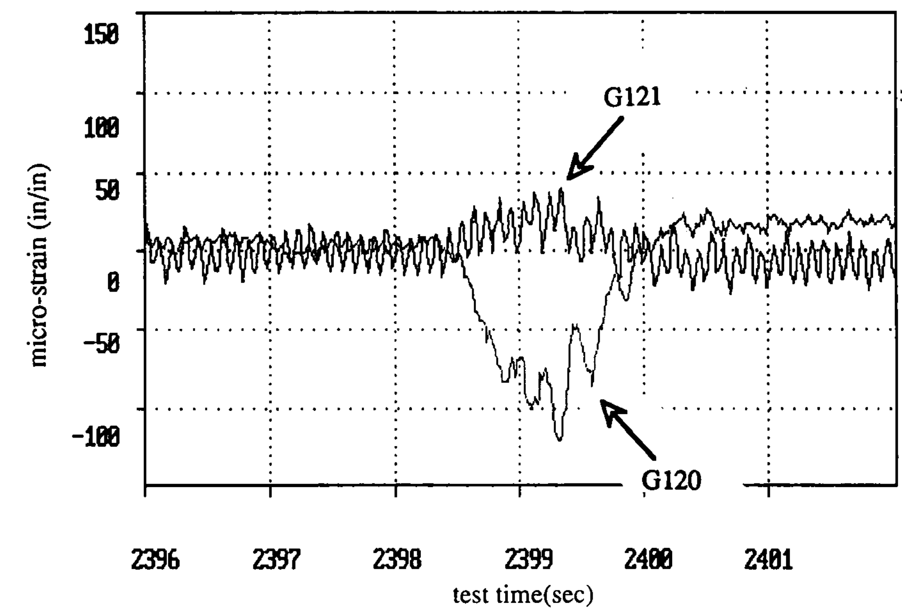

Figure 4.13 - Strain responses for gages 105 and 106 due to a 3S2 truck - east bound middle lane

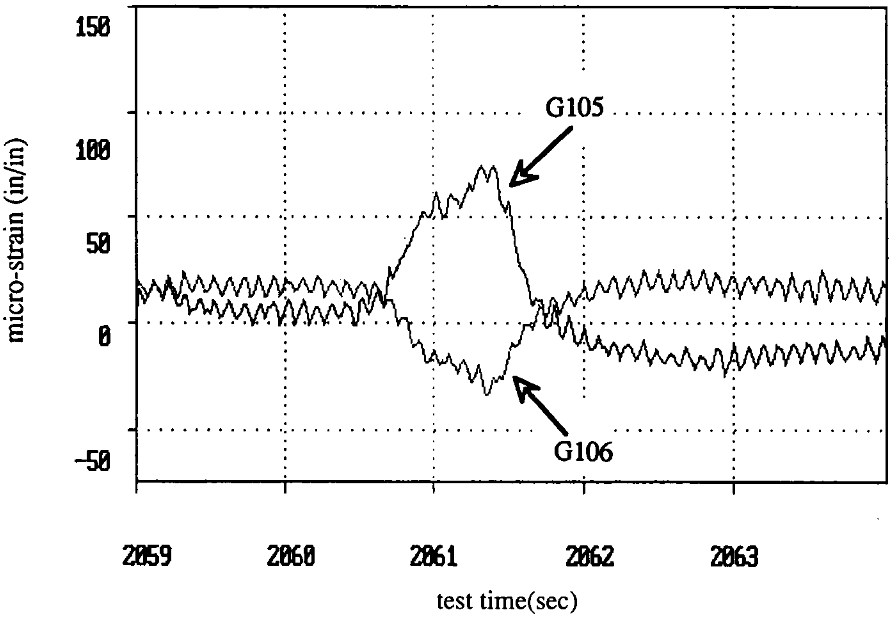

Figure 4.14 - Strain responses for gages 105 and 106 due to a 3S2 truck - east bound right lane

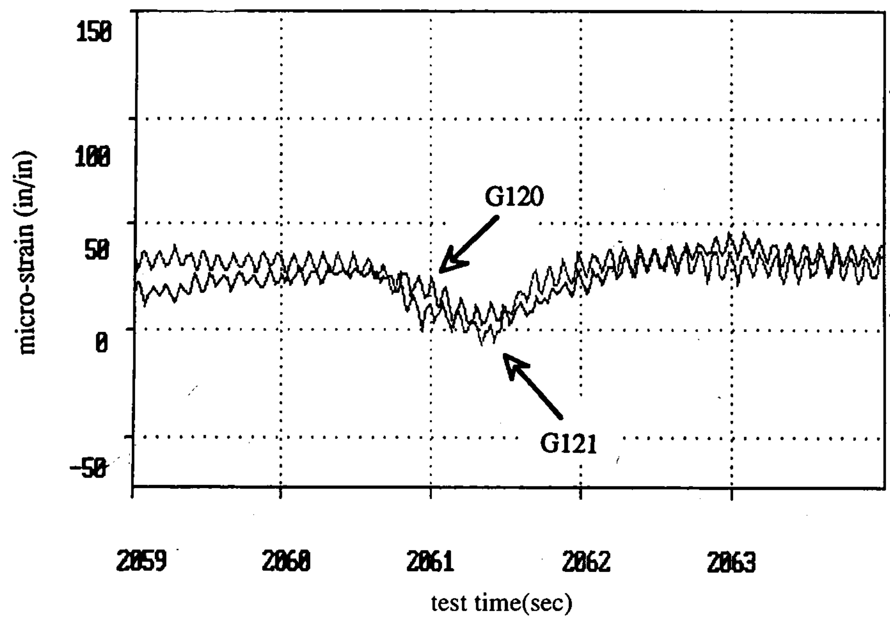

Figure 4.15 - Strain responses for gages 120 and 121 due to a 3S2 truck - east bound right lane

Table 4.1 - Comparison of measured versus calculated stresses

Lane Loading Cond.	Stress (ksi) at Gage Location No.											
	G105			G106			G120			G121		
	msrd.	calculated		msrd.	calculated		msrd.	calculated		msrd.	calculated	
		fixed	semi-rigd		fixed	semi-rigd		fixed	semi-rigd		fixed	semi-rigd
Westbound												
Right	0.15(+)	0.63(+)	0.66(+)	0.30(-)	0.35(-)	0.70(-)	0.70(+)	0.48(+)	0.5(+)	0.70(-)	1.6(-)	1.8(-)
Middle	0.78(-)	1.55(+)	1.73(+)	0.49(-)	0.69(-)	1.30(-)	3.48(+)	6.0(+)	6.3(+)	0.87(-)	3.6(-)	3.35(-)
Left	0.73(-)	1.1(+)	2.1(+)	0.36(-)	0.65(-)	1.14(-)	4.35(+)	14(+)	13.0(+)	0.87(-)	3.2(-)	3.3(-)
Eastbound												
Left	0.50(-)	6.3(-)	5.5(-)	1.60(+)	2.5(+)	5.8(+)	4.06(-)	2.1(-)	4.6(-)	1.30(+)	12(+)	11.4(+)
Middle	1.74(+)	1.8(+)	1.2(+)	0.16(-)	0.70(+)	1.74(+)	3.0(-)	4.9(-)	4.4(-)	0.56(+)	2.4(+)	3.35(+)
Right	2.10(+)	4.2(+)	2.8(+)	1.10(-)	1.11(-)	2.26(-)	0.75(-)	1.6(-)	0.9(-)	1.0(-)	4.8(-)	3.75(-)

Notes: (+) indicates tension
(-) indicates compression.

stresses. The model was run using a "fixed" girder-floor beam connection and a "semi-rigid" connection. The stress values for both conditions were calculated for the six lane loading conditions depicted in figure 4.16. The two concentrated loads were determined to be the static equivalent of the live and impact wheel loads of the 3S2 trucks which caused the measured stresses (Appendix B). The model was run for each loading condition and the stress distributions were obtained. The resultant stresses at the gage locations are tabulated in Table 4.1.

The comparison of calculated versus measured stresses shows that the calculated stress magnitudes were consistently larger. This was expected since a "fixed" floor beam connection will have a larger bending moment and therefore greater stresses.

The west bound middle and left lane loadings of the measured stresses produced some unexpected results. These loadings consistently caused compressive stresses at gages 105 and 106 during the passage of a 3S2 truck. It was expected that the stresses would be opposite in sign. These stress results indicate that there was a large amount of compressive stress in the bottom and a small amount of tensile stress in the top of the center floor beam. Since this floor beam was 5.0 inches higher in elevation than the outer floor beams, the compressive stress was transferred to the outer floor beam, while the tensile stress was transferred to the girder web connection.

4.3 Interpretation of Floor Beam Stress Results

A series of qualitative conclusions can be made from the interpretation of the measured and calculated stress results:

1) Bending, caused by differential girder deflection, produced significant stress concentrations at the coped flanges. This was due to the partial fixity of the floor beam

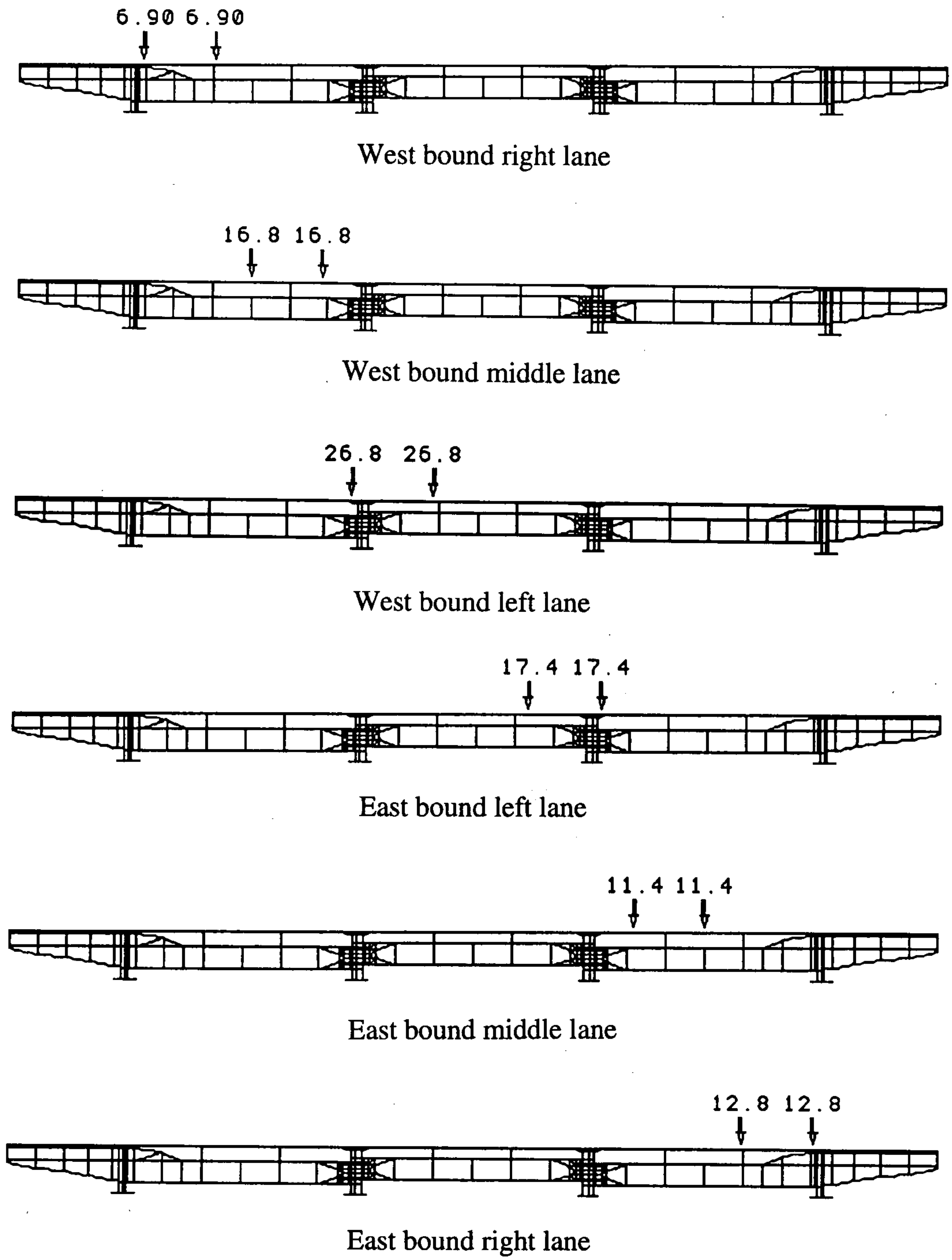

Figure 4.16 - Lane loading conditions with an equivalent truck for the calculated stresses

connection and the reduction in section modulus at the coped flange.

2) Gages 105 and 120 exhibited stress ranges of magnitudes greater than gages 106 and 121, respectively, since the bottom portion of the transverse connection plate has greater lateral displacement than at the top during an applied load. This is due to the higher end restraint of the girder-deck composite action and the floor beam web-girder connection plate top flange weldment. The higher end restraint can be seen in figure A.10, where the bottom flange of the girder exhibits lateral displacement during an applied load.

3) Gage 106 exhibited stress ranges of lower magnitude than gage 105. Some of the bending stress in the floor beam bottom flange is transferred to the lateral gusset plate connection, thereby lowering the stress at gage 106.

4) Gages 103 and 104 did not exhibit significant stresses due to the knee stiffeners and the lateral gusset plate connection.

All of these conclusions were expected from knowledge of the floor beam design and were exhibited by the measured and calculated stresses. This indicates that the measured stress data used in the fatigue life estimation of the floor beam were reliable.

4.4 Estimation of the Remaining Floor Beam Fatigue Life

The remaining fatigue life estimates of the floor beams were compiled in Tables 3.1 and 3.2. The estimates indicated that a fatigue crack should have started to propagate in the center floor beam at the location of Gage 120 approximately seven to eight years ago. There are two reasons why a crack has not appeared, each involving conservative assumptions used throughout the fatigue life calculations:

1) The AASHTO fatigue design tables which relate the stress range, S, to the number of cycles, N, which can be resisted, were derived from test data. The tables, as described in the literature review, are derived to expect that 97.5% of the experimental data would

survive. The floor beam is obviously within the 97.5% category.

2) The procedure used to estimate the fatigue life of the floor beam was based on the nominal stress range, neglecting stress concentrations caused by the flange cope and partial fixity of the beam. None of the gage locations precisely meet this condition. The stress concentration created by the flange cope will increase the measured effective stress ranges, thereby decreasing the estimated remaining life.

There were also sources of uncertainty in calculating the stress history:

1) The first was the uncertainty in the number of cumulative cycles, N_p, the floor beams have experienced to date. This value was determined from a linear extrapolation of data collected from present day and past traffic estimates, all of which required assumptions.

2) The second source of uncertainty was the correlation of the number of cycles generated by a number of trucks at an effective stress range. Present day data were used to determine the effective stress range and the number of cycles per truck, whereas, in actuality these values have varied over the history of the bridge, since the truck traffic characteristics have been changing. The tendency has been toward a greater number of 3S2 trucks, hence heavier loads. There have also been increases in the legal truck weight limit from 72,000 to 80,000 pounds. These changes will result in a higher number of cycles per truck and a higher effective stress range used in the fatigue life estimates.

The estimates for the gage locations of 106 and 121 indicate that there is no potential fatigue problems, since all the stress ranges are below the fatigue limit, F_{sr}, for a category E detail (4500 psi). Even though only a limited amount of data was collected over a brief period of time, the estimates are probably valid. Any additional data collected is likely to result in stress ranges greater than 4500 psi, especially at gages 106 and 121.

Although the fatigue estimates are based on conservative assumptions and fatigue cracks at the instrumented locations have not yet appeared, the fatigue life estimation was made in accordance with the "State of the Art" Bridge Fatigue Estimation techniques (8) and engineering judgment. Also, fatigue cracks have developed at the floor beam web copes in the third span of the bridge.

Chapter 5

Summary

It was the objective of this thesis to: 1) study the critical details on the floor beams for potential fatigue problems; 2) analyze the stress data; and 3) estimate the remaining fatigue life of the floor beams based on the current and estimated future usage. The conclusions are summarized as follows.

1) Floor Beam Critical Details - The results indicate that significant stresses developed at the floor beam copes which cause fatigue problems. The stresses were caused by the combination of girder differential deflection, partial fixity of the floor beam, and flange coping. The elimination of coping is the simplest method of reducing potential fatigue problems in design, for the three causes mentioned above. In the design of the bridge floor beams, a simple span was assumed with only shear being transmitted to the girder through the bolted connection. Therefore, the only requirement was to design for shear. The simple span assumption is considered beneficial since it provides a conservative design, and any partial fixity in the floor beam will increase the moment capacity. However, the coping (i.e., reduced section modulus) in conjunction with the partial fixity of the connection providing an applied stress range (moment) may cause fatigue cracking.

An acceptable floor beam to girder connection is shown in figure 5.1 (24), in which only half of the flange is removed from the section. Here the connection provides a more gradual reduction in the section modulus.

2) Data Results - A total of 7.25 hours of test data was analyzed from the strain gages on the floor beams. The data was categorized using the Rainflow and Mean Crossing Peak methods. The stress range spectrums determined from the two methods are shown in

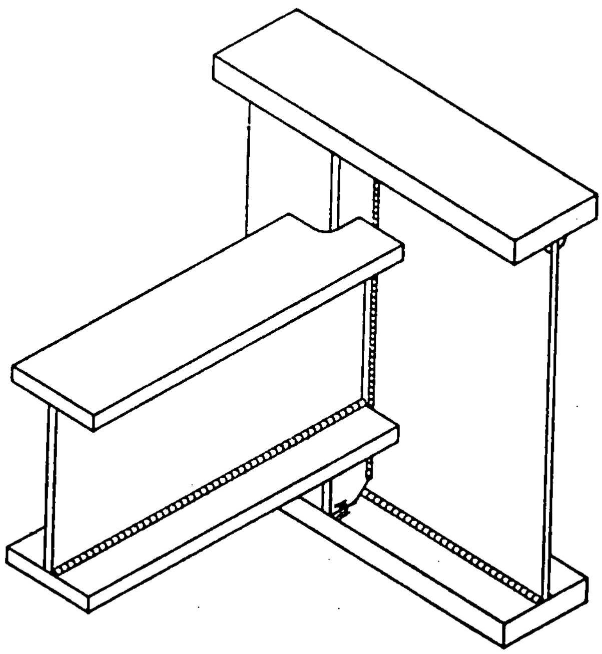

Figure 5.1 - Acceptable floor beam to girder connection detail

figures 3.5 through 3.12. At each gage location the spectrums were similar, which provides an indication that the data are consistent and reliable. However, the total number of stress range counts varied from 10% to as much as 50% due to the differences in the two counting methods.

The Rainflow counting method counts half cycles, which significantly increases the number of stress range counts at magnitudes less than 1000 psi. These lower stress ranges were deleted from the data. The deletion results in an increased effective stress range for both counting methods, but to a much greater degree for the Rainflow method. These two factors of decreased stress cycles and increased effective stress range tend to offset each other. Therefore, the two counting methods did produce similar fatigue life estimates.

In an effort to verify the measured stresses, a 2-D model of the floor beam was used to calculate the stresses at the gage locations. In all loading conditions, the calculated stresses were greater than the measured stresses. The differences ranged from 10% to 1000%. The inaccuracy may have been due to the modeling of a "fixed" connection. Attempts were made to model the connection as a "semi-rigid" connection which led to stresses of approximately the same values. The inaccuracy from both models may be due to a greater distribution of the truck loads to the adjacent girders and floor beams in the actual bridge. There may also be inaccuracy in the determination of the equivalent loads. The 2-D model did however verify the behavior and the locations of stress concentrations at the critical details.

3) Fatigue Life Estimate - Using very conservative methods and assumptions, it was shown that the floor beams are likely to develop fatigue cracks at the present time. The inspection program by the State DOT should pay particular attention to the floor beam

flange-web fillet weld at the coped flange locations.

List of References

1. American Association of State Highway and Transportation Officials, AASHTO Standard Specifications for Highway Bridges, 14th Edition, 1989.

2. Deatherage, J. Harold, Proposal for the Investigation of the Fatigue Life of the I-40 Bridge over the Holston River, Knox County, State of Tennessee Department of Transportation Planning Division, March 17,1993.

3. Dowling, N.E., Fatigue Failure Predictions for Complicated Stress-Strain Histories, Journal of Materials, JMLSA, Vol. 7 no. 1 March 1972, pp71-87.

4. Federal Highway Administration Publication No. FHWA-RD-89-167, Fatigue Cracking of Steel Bridge Structures, Volume II, March 1990.

5. Fisher, J.W., B.T. Yen and D. Wang , Fatigue of Bridge Structures- A Commentary and Guide for Design, Evaluation and Investigation for Cracking, ATLSS Report No. 89-02, NSF-ERC Advanced Technology for Large Structural Systems, LeHigh University, Federal Highway Administration Research Report FHWA-RD-89-167.

6. Fisher, J.W., B.T. Yen, D. Wang and J.E. Mann., Fatigue, Fracture Evaluation for Rating Riveted Bridges, Fritz Engineering Laboratory #499.3, Bethlehem, PA 1988; NCHRP Report #302, Transportation Research Board, December 1987.

7. Fisher, John W., Inspecting Steel Bridges for Fatigue Damage, Lehigh University: Fritz Engineering Laboratory #386-15(81), Report #72-3 FHWA/PA-81/005, March 1981.

8. Fisher, John W., Ti Tiuang, Lung-Yang Lai and Ben T. Yen., Manual for Inspecting Bridges for Fatigue Damage Conditions, Lehigh University: Dept. Civil Engineering #511-1, Report #FHWA-PA-89-022+85-02, January 1990.

9. Goodpasture, David W., Final Report on Stress History of Highway Bridges-II, University of Tennessee, June 30, 1976.

10. Gurney, T.R., Fatigue of Welded Structures, Second Edition, Cambridge University Press, 1979.

11. Hahn, C., J.M. South, J. Mohammedi, R.K. Polepeddi, Accurate and Rapid Determination of Fatigue Damage in Steel Bridges, Jnl. of Structural Engineering, vol. 119 no. 1, Jan. 93.

12. Hanson, J.M., M.J. Koob, and J.W. Fisher, Evaluation of Fatigue Life and Retrofitting on the Bencia-Martinez Bridge, Transportation Research Board 1290.

13. Hulsbos, C.C. and D.A. Linger, Dynamic Tests of a Three Span Continuous I-Beam Highway Bridge, HRB Bulletin 279, 1961, pp. 18-46.

14. Keating, P.B. and J.W. Fisher, Review of Fatigue Tests and Design Criteria on Welded Details, Fritz Engineering Lab Report 488-1(85), Lehigh University, Bethlehem, PA, Oct. 1985.

15. Layout of Bridge I-40 Over the Holston River and Station 785+15 Knox County:

Drawing K-100-119, State of Tennessee Department of Highways. 1970.

16. Mayhew, Mark D., Measured Stress Ranges and Cross Frame Analysis of the Holston River Bridge, Masters thesis, The University of Tennessee, May 1994.

17. Miner, M.A., Cumulative Damage in Fatigue, Journal of Applied Mechanics, Vol. 121, Sept. 1945, pp. A-159.

18. Moses, F., C.G. Schelling and K.S. Raju, Fatigue Evaluation Procedures for Steel Bridges, NCHRP Report no. 299, Transportation Research Board, December 1987.

19. Optim Corporation, Technical Manual for the Megadac Series 3000, Optim Corporation, Release 1.0 May 1982.

20. Sanders, M.D., Controlled Load Tests on a Four Girder Steel Bridge, Masters Thesis, The University of Tennessee, Knoxville TN, May 1994.

21. Schilling, C.G., Klippstein, K.H., Barsom, J.M., and Blake, G.T., Fatigue of Welded Steel Bridge Members Under Variable Amplitude Loading, NCHRP Report 188, Transportation Research Board, 1978.

22. Tennessee Department of Transportation, City and County Traffic Maps showing average daily traffic, 1974-1992.

23. 8 Span Continuous Welded Steel Girder Bridge on I-40 over Holston River and SR168, Knox County(47): Inspection Report, Br#47-I40-25.92.

24. Federal Highway Administration Publication Number FHWA-HI-90-043, Economical and Fatigue Resistant Steel Bridge Details, October 1990.

Appendices

Appendix A

Floor Beam Model

The floor beam cross section was modeled using a finite element program called GTSTRUDL (Georgia Tech STRUctural Design Language). The program has the capability to generate contours of principal stress distributions and calculate principal stresses. This provided a method for identifying stress concentrations and approximating stress magnitudes for each lane loading condition.

In the development of the model, the boundary conditions consisted of a spring constant at the bottom of each girder to account for girder deflection. The spring constant value of 69.2kips/inch was calculated using GTSTRUDL (20). The floor beam and girders were run in plane stress using "Iso-Parametric Quadrilateral Quadratic Displacement" elements, with a steel modulus of elasticity equal to 29,000 ksi. The 7.5 inch concrete deck (E=3500 psi) was run as plane frame members and attached to the girders and floor beams by rigid links.

The modeled structure is depicted below:

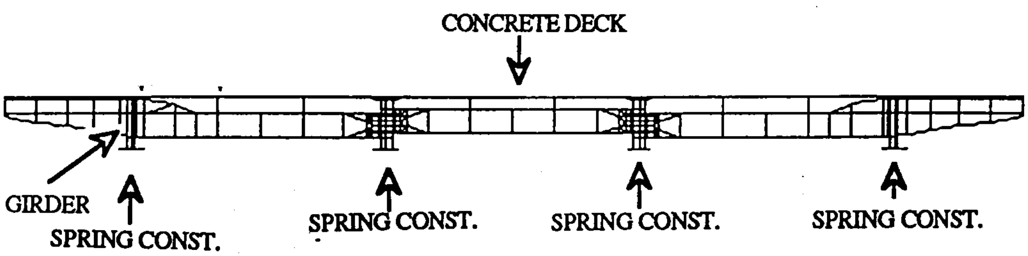

Figure A.1 - Floor beam model

The floor beam girder connection was modeled under two conditions. The first utilized the assumption of a "fixed" connection. The finite element mesh used for the connection is shown in figure A.2. The structure was loaded in the six lane loading conditions as shown in figure 4.15. The resultant stresses are listed in table 4.1. The second condition involved an attempt to model the connection as a "semi-rigid" connection. A detail of the finite mesh is depicted in figure A.3. The results are listed in table 4.1. The stress distributions for each lane loading condition are depicted in figures A.4 through A.9. An example of a deformed structure with a magnification of 134 times is shown in figure A.10.

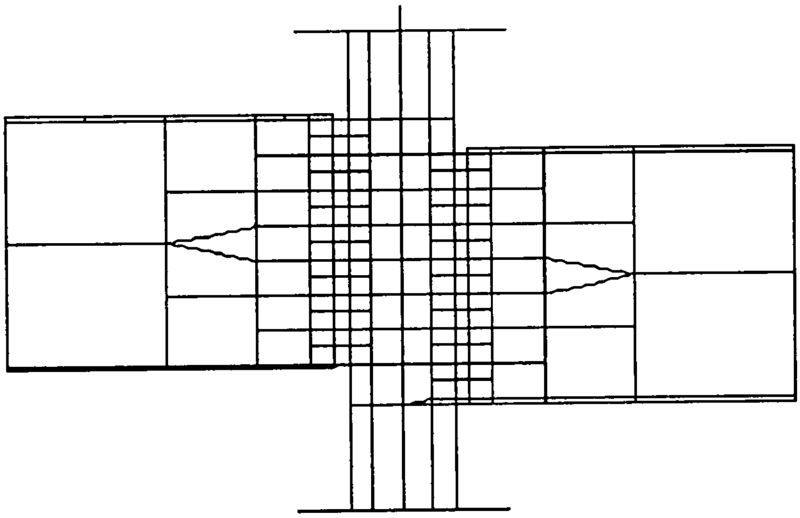

Figure A.2 - Finite element mesh for “fixed” floor beam-girder connection

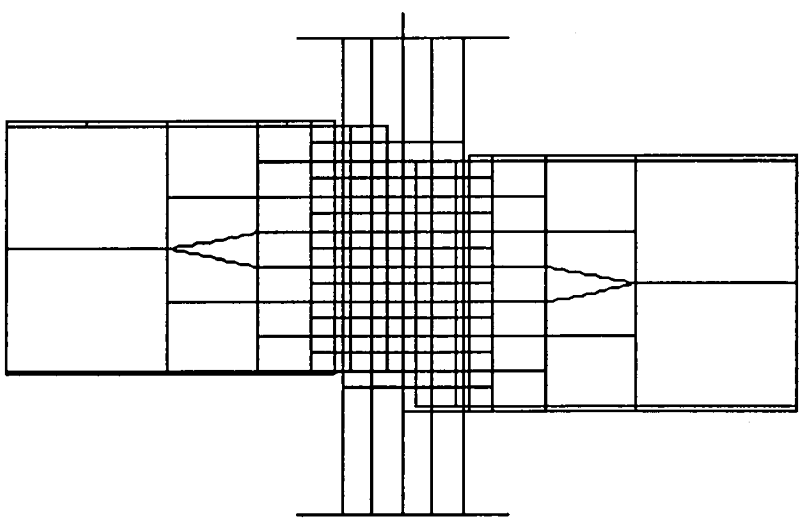

Figure A.3 - Finite element mesh for “semi-rigid” floor beam-girder connection

```
SXX MID CONTOUR STEP 0.300000 KIP/IN**2
LD 1   MIN - 2.5776   MAX   1.0905
>
                    Y
                    |        24.5714 HORIZONTAL IN UNITS PER INCH
                    |___X    24.5714 VERTICAL IN UNITS PER INCH
                          ROTATION:  Z   0.0  Y   0.0  X   0.0
```

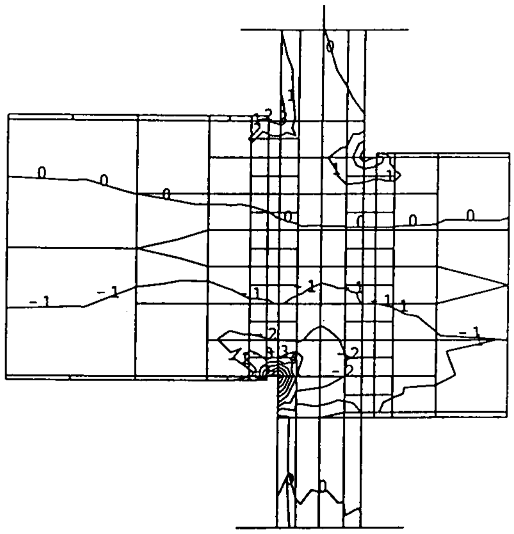

Figure A.4 - Stress distribution of floor beam connection due to a 3S2 truck - west bound right lane

```
SXX MID CONTOUR STEP 1.200000 KIP/IN**2
LD 2   MIN - 5.5563   MAX   11.2405
>
                    Y
                    |        23.4286 HORIZONTAL IN UNITS PER INCH
                    |___X    23.4286 VERTICAL IN UNITS PER INCH
                          ROTATION:  Z   0.0  Y   0.0  X   0.0
```

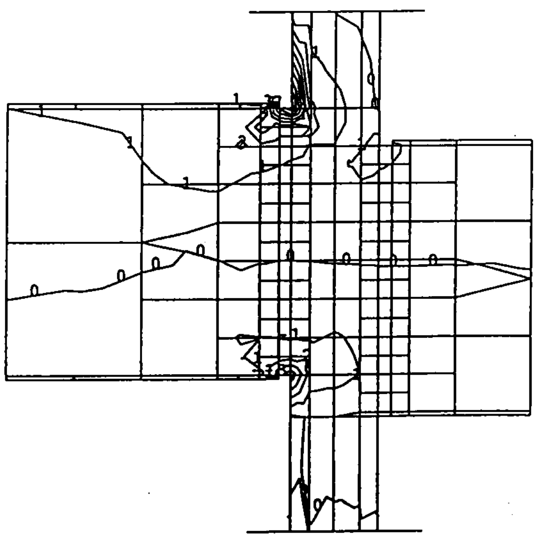

Figure A.5 - Stress distribution of floor beam connection due to a 3S2 truck - west bound middle lane

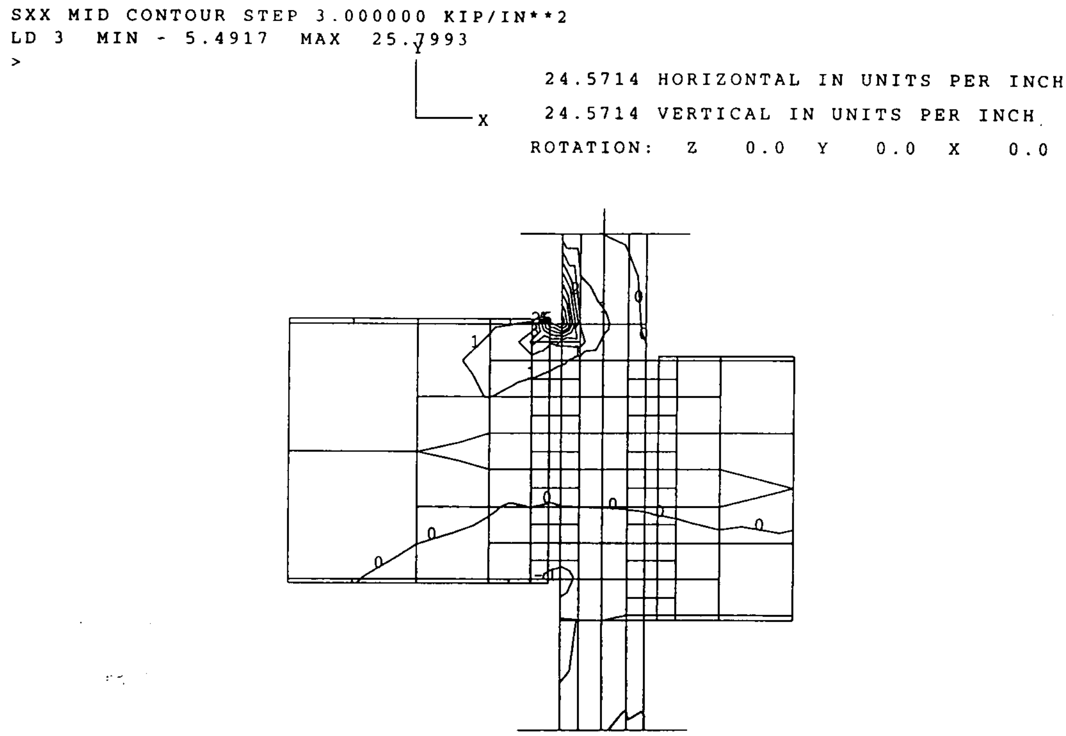

Figure A.6 - Stress distribution of floor beam connection due to a 3S2 truck - west bound left lane

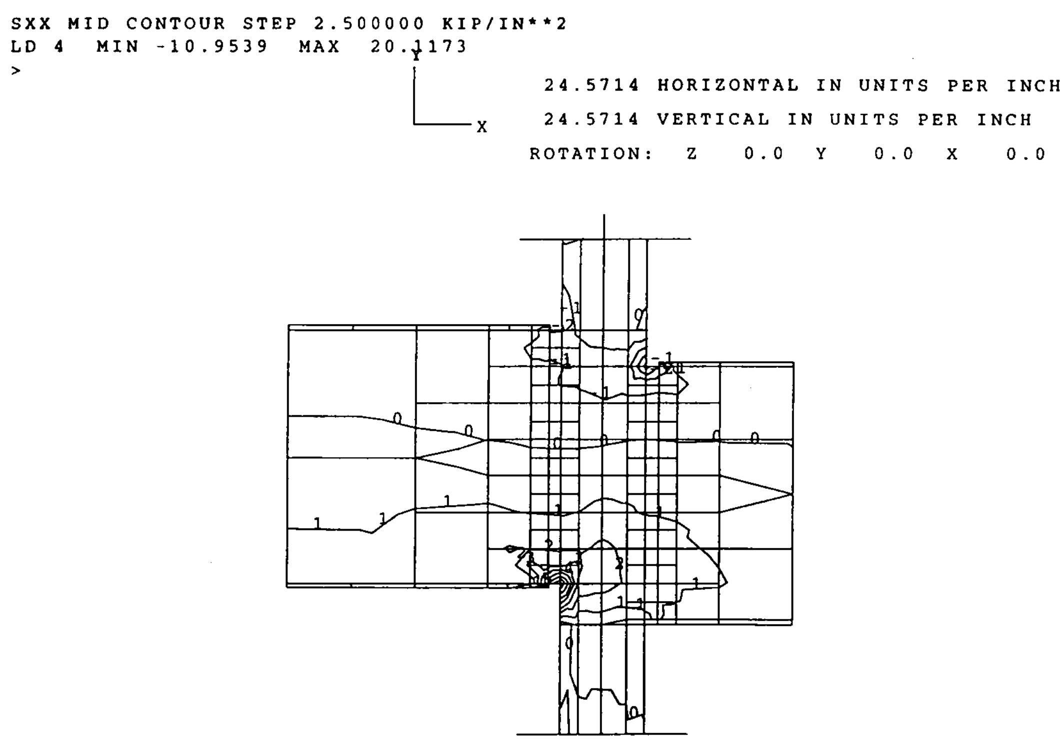

Figure A.7 - Stress distribution of floor beam connection due to a 3S2 truck - east bound left lane

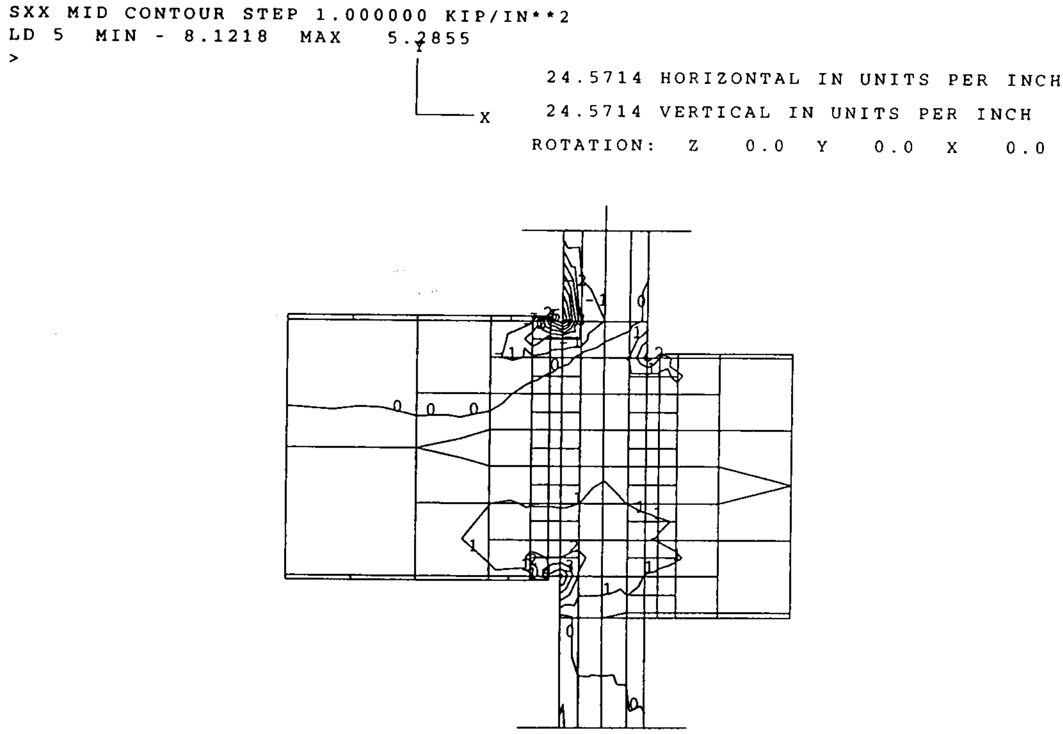

Figure A.8 - Stress distribution of floor beam connection due to a 3S2 truck - east bound middle lane

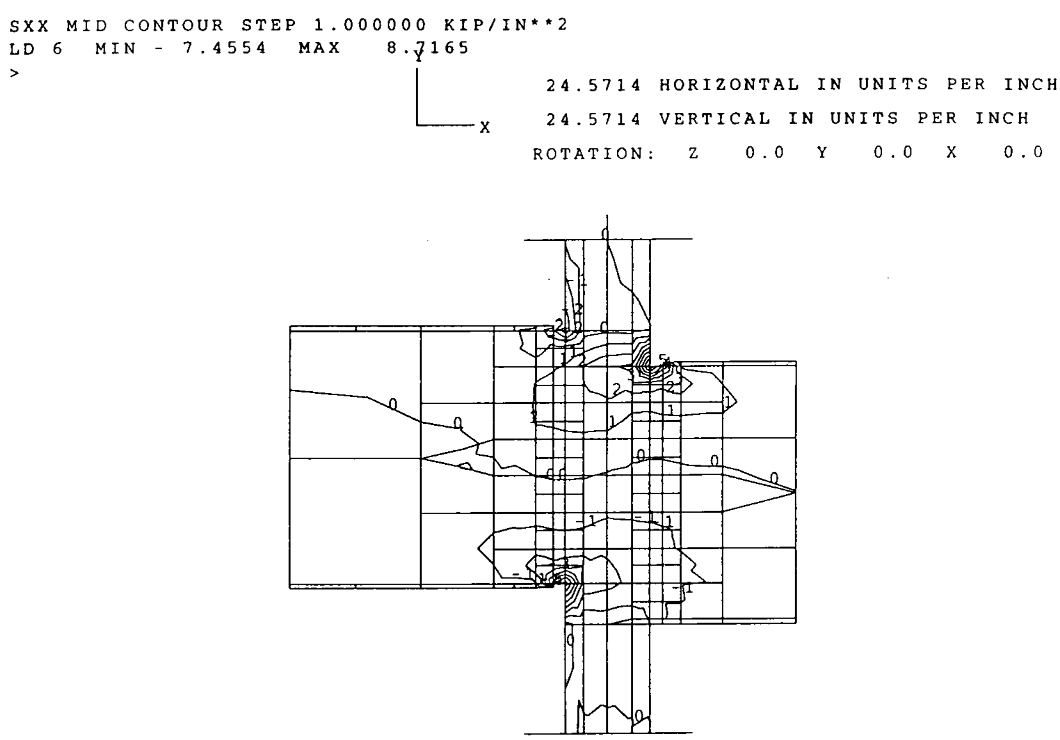

Figure A.9 - Stress distribution of floor beam connection due to a 3S2 truck - east bound right lane

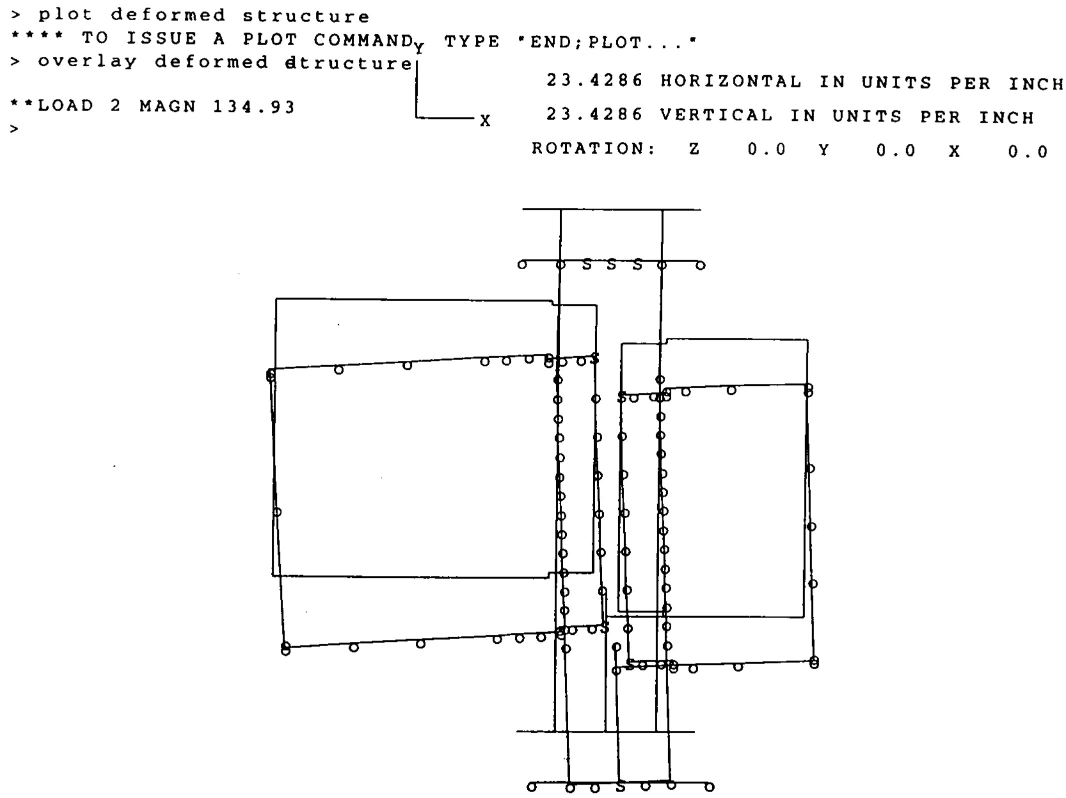

Figure A.10 - Deformed structure at floor beam connection due to a 3S2 truck - west bound middle lane

Appendix B

Determination of Equivalent Loads for the 2-D Model

Equivalent loads to be placed on the 2-D model had to be determined in order to compare calculated with the measured stresses. In the measured floor beam stress responses (figures 4.3 through 4.14), the gross vehicle weights of the 3S2 trucks were unknown. Also, the floor beam strain gage responses were not evaluated during the controlled load tests (20). Therefore, equivalent loads were determined using the responses of gages located at the bottom of the girder flange (G30 and G83). These responses were measured during both the controlled load tests and during the floor beam stress tests. A ratio of these values can be used to estimate the load which caused the measured floor beam stresses. The procedure used was as follows:

1. The test truck was a 3D type truck of gross weight 77 kips. The test truck load was positioned longitudinally along the influence line of a girder span for a maximum reaction at the floor beam location. The maximum reaction was determined to be 54 kips from moment distribution.

2. The 54 kip load was ratioed with the stress responses of the girder gages (G30 and G80) during the controlled load and floor beam tests. Using this ratio, an equivalent load can be estimated from any measured stress response in gages G30 and G80, where

$$\text{Equivalent Load} = \frac{\text{54 kips x Floor Beam Stress Response}}{\text{Controlled Load Stress Response}}$$

These equivalent loads were then used for each of the lane loading conditions as shown in figure 4.15.

A summary of the calculations is shown in the table B.1 below:

Table B.1 - Determination of equivalent loads

	Lane (Gage 83 Stress Response) west bound			Lane (Gage 30 Stress Response) east bound		
	right	middle	left	left	middle	right
A. Controlled Load Tests (ksi) (=A)	2.61	1.85	1.17	1.35	2.13	3.19
B. Floor Beam Tests (ksi) (=B)	0.667	1.102	1.16	0.87	0.899	1.508
D. Equivalent Load(kips) (=54xB/A)	13.80	32.17	53.54	34.80	22.79	25.53
E. Wheel Load(kips) (=D/2)	6.90	16.08	26.77	17.40	11.40	12.76

Vita

Marc Anthony Matulich was born on December 2, 1961 in Santa Monica California. He attended high school at Rolling Hills High School in California and graduated in June of 1979. The following September he entered the University of California at Santa Barbara. In June of 1983 he received his Bachelor of Science degree in Nuclear Engineering. In January 1993, he entered the University of Tennessee at Knoxville as a graduate student in Civil Engineering. He became a graduate assistant in Civil Engineering in January 1994. Approximately one and one half years later he graduated with a Master of Science degree in Civil Engineering in May of 1995.